(20)

A TRIDENT SCHOLAR PROJECT REPORT

NO. 196

"INVESTIGATION OF A POSSIBLE GALACTIC CHIMNEY"

UNITED STATES NAVAL ACADEMY
ANNAPOLIS, MARYLAND

071

U.S.N.A. - Trident Scholar project report; no. 196 (1992)

"INVESTIGATION OF A POSSIBLE GALACTIC CHIMNEY"

A Trident Scholar Project Report

by

Midshipman Bonnie R. Roberts, Class of 1992

U.S. Naval Academy

Annapolis, Maryland

Carol Elise Albert

Adviser: Associate Professor C. Elise Albert
Physics Department

Doctor Laura Danly
Space Telescope Science Institute

Accepted for Trident Scholar Committee

Francis D'Correcc

Chair

8 May 1992

Date

REPORT DOCUMENTATION PAGE

Form Approved
OMB No 0704-0188

1. AGENCY USE ONLY (Leave blank)	2. REPORT DATE	3. REPORT TYPE AND DATES COVERED
	8 May 1992	Final 1991/92

4. TITLE AND SUBTITLE

INVESTIGATION OF A POSSIBLE GALACTIC CHIMNEY

5. FUNDING NUMBERS

6. AUTHOR(S)

Roberts, Bonnie R.

7. PERFORMING ORGANIZATION NAME(S) AND ADDRESS(ES)

U.S.Naval Academy, Annapolis, Md.

8. PERFORMING ORGANIZATION REPORT NUMBER

U.S.N.A. - TSPR;
196 (1992)

9. SPONSORING/MONITORING AGENCY NAME(S) AND ADDRESS(ES)

10. SPONSORING/MONITORING AGENCY REPORT NUMBER

11. SUPPLEMENTARY NOTES

Accepted by the U.S.Trident Scholar Committee

12a. DISTRIBUTION/AVAILABILITY STATEMENT

This document has been approved for public release; its distribution is UNLIMITED.

12b. DISTRIBUTION CODE

13. ABSTRACT (Maximum 200 words)

Since the discovery in 1924 that we live in a separate star system, now known as the Milky Way Galaxy, astronomers have worked to understand the structure, composition and dynamics of our galaxy. A particular puzzle in recent years has been the origin and dynamics of the interstellar gas in the halo region of the galaxy high above the visible flat stellar disk. The chimney model dominates current theories of the source, support and ionization of the halo gas, yet no one has actually seen a galactic chimney. The most likely candidate for a galactic chimney in our galaxy was observed. The National Radio Astronomy Observatory telescope and NASA's International Ultraviolet Explorer satellite were used in these observations. The observations provided the data for the study. The investigation take the approach of observing a single region in great detail at many different wavelegnths in order to gain understanding of the composition, ionization, and dynamics of the halo gas in the region of a possible galactic chimney.

14. SUBJECT TERMS

interstellar matter; galaxies; Milky Way

15. NUMBER OF PAGES

73

16. PRICE CODE

17. SECURITY CLASSIFICATION OF REPORT	18. SECURITY CLASSIFICATION OF THIS PAGE	19. SECURITY CLASSIFICATION OF ABSTRACT	20. LIMITATION OF ABSTRACT
UNCLASSIFIED	UNCLASSIFIED	UNCLASSIFIED	

Table of Contents

ABSTRACT

Since the discovery in 1924 that we live in a separate star system, now known as the Milky Way Galaxy, astronomers have worked to understand the structure, composition and dynamics of our galaxy. A particular puzzle in recent years has been the origin and dynamics of the interstellar gas in the halo region of the galaxy high above the visible flat stellar disk. The "chimney model" dominates current theories of the source, support and ionization of the halo gas, yet no one has actually seen a galactic chimney. We selected the most likely candidate for a galactic chimney in our galaxy and observed the candidate region with both emission and absorption spectra over a wide wavelength range. We were granted observation time to observe radio wavelength emission spectra with the 140 foot National Radio Astronomy Observatory telescope at Green Bank, West Virginia, and ultraviolet absorption spectra with the National Aeronautics and Space Administration's International Ultraviolet Explorer satellite. These original observations, combined with previous observations in radio, optical and ultraviolet wavelengths, provided the data for the study. The investigation takes the novel approach of observing a single region in great detail at many different wavelengths in order to gain understanding of the composition, ionization and dynamics of the halo gas in the region of a possible galactic chimney.

I Introduction

Our galaxy is a spiral galaxy like many of its neighbors (Figure 1). The Sun resides about 8.5 kpc (1 parsec (pc)= 3.086×10^{16} m = 3.26 light years) from the galactic center along one of the spiral arms, and the total galactic diameter extends approximately 50kpc. The galaxy rotates about its mass centroid located in the dense inner galactic nucleus. A nearly spherical mass of stars

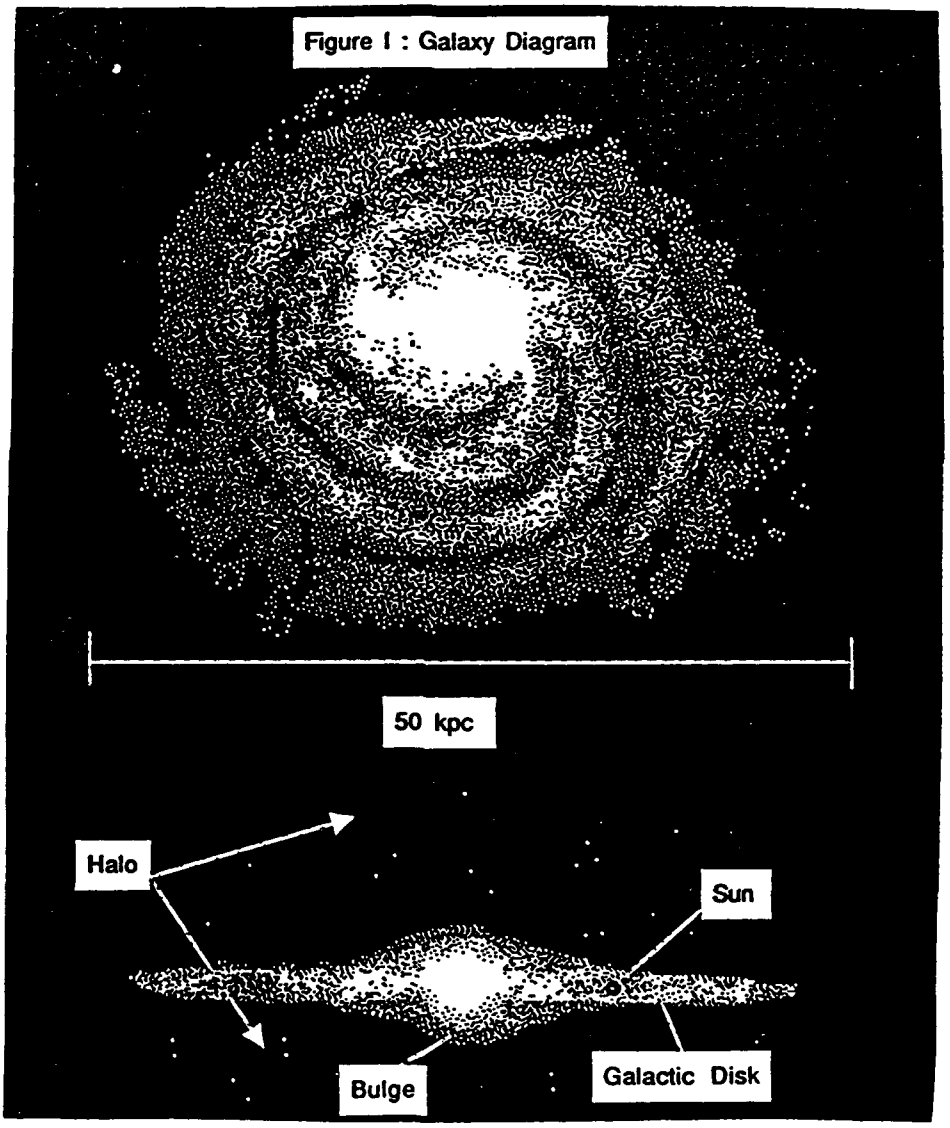

Figure 1: Upper: a spiral galaxy seen face-on to the disk. Lower: a spiral galaxy seen edge-on to the disk.

called the bulge surrounds the nucleus. The dense region in the plane of the galaxy containing the spiral arms is known as the galactic disk while the space extending far above and below the disk and containing only a sprinkling of stars is called the galactic halo.

Vast clouds of gas and dust lie between the stars in the galactic disk and total about one tenth of the mass of the galaxy. Often the gas is diffuse but occasionally gas is also found in dense nebular clouds, such as the Great Nebula in Orion, that shine brilliantly when lit by nearby stars. One particularly interesting question is how stars and interstellar material are related. The stars in the Milky Way appear to have grouped by age with the older (Population II) stars generally found in the halo and bulge and the younger (Population I) stars in the spiral arms of the disk. Within the spiral arms, the interstellar gas and dust experience the pressure required to form new stars. When very massive stars die (run out of effective fuel to maintain fusion), they explode violently in a supernova. With tremendous force, the star throws out the gas that once comprised it into the surrounding area of the galaxy where the gas eventually becomes recycled into new stars. Because the heavier elements only form within stars and during the supernova explosion, the composition and metal content of the gas tells much about its history.

While most of the interstellar gas appears concentrated in the disk, interstellar clouds of both neutral and ionized gas have been observed high above the plane of the galaxy (Munch and Zirin 1961; Albert 1983; Albert el.al. 1992; Danly 1989), inspiring many questions about its support (what keeps the gas up), ionization (the degree to which the atoms have lost electrons, either from absorbing photons or from collisions), and kinematics (how the gas moves around).

Two major theories have developed explaining the support and ionization of halo gas. In the "cold halo" theory, cosmic ray pressure provides the support, and ionization occurs through photoionization (Chevalier and Fransson 1984). This is to say that the pressure exerted by high energy charged particles supports the gas and energy imparted by the light from various sources ionizes the gas while no energy is extracted from thermal means. In an opposing theory, the "hot halo" theory, both support and ionization are achieved by thermal means. Heated gas rises from the disk into the halo and then cools into clouds which fall back into the disk completing the cycle known as a galactic fountain (Shapiro and Field 1975; Bregman 1980).

The galactic chimney model explains one possible outflow mechanism of the fountain model. The chimney theory proposes that correlated groups of supernovae in the disk form "superbubbles" (Heiles 1986, 1987) of hot, ionized gas, which may expand until they break out of the dense disk gas into the halo, thus forming a conduit or "chimney" of hot, ionized gas between the disk and the halo. The gas then cools and rains back into the disk as in other fountain models (Norman and Ikeuchi 1989). Figure 2 illustrates the chimney model.

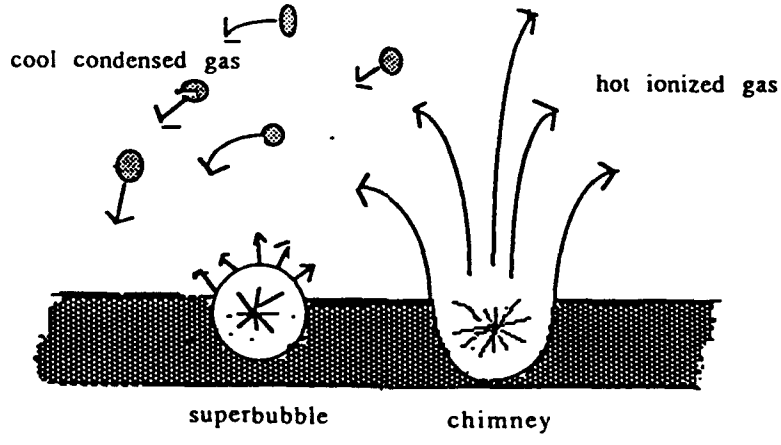

Figure 2: A qualitative illustration of the dynamic cycle of a galactic chimney.

While the chimney theory has been well developed, no one has actually seen a galactic chimney. We explored one region of the galaxy where a chimney may likely be located. Two methods to study gas in the halo are to observe emission spectra of neutral hydrogen and to observe the absorption spectra of other ions against background stars. The bulk of the interstellar gas is neutral hydrogen (H I), which is observed directly in emission, giving a "glow" brighter than the background radiation at the radio wavelength of 21 centimeters. Other less abundant species, such as calcium and titanium, are mixed with the hydrogen and are observed in absorption. Looking at absorption spectra is somewhat analogous to using a silhouette (at a given wavelength) against the light from a distant star to get information about the matter in front of the star. Velocities of the gas are determined by its Doppler shift where the ratio of the change in the wavelength at which we observe a spectral line to the actual wavelength equals the ratio of the velocity of the gas to the speed of light ($\Delta\lambda / \lambda = v / 3x10^5$ km/s). Study of the gas at many different wavelengths (and therefore many different energies) reveals much about the physics of the gas, giving a much more complete picture than any one wavelength could show.

Cold neutral hydrogen clouds at a temperature of about 100 K are observed with radio telescopes, while optical telescopes can detect trace element absorption both from cold and from warmer ionized gas at 10,000 K. However, because of their atomic structure, most chemical elements produce strong absorption in the ultraviolet region of the spectrum and can be studied over a wide temperature range of 100 K to 200,000 K with orbiting ultraviolet satellites. We must use all of these techniques to search for a possible galactic chimney.

II The Investigation

Based on the optical and ultraviolet absorption studies of Albert and Blades et. al. (1992) and Danly (1989), we selected the most probable location of a galactic chimney in our galaxy: the region around the famous halo star HD119608. A number of unusual characteristics makes this the best region for this study. This is the only area to show a marked outflow of gas in low ion (neutral and singly ionized) absorption spectra and in H I emission. At the same time as we see unusual outflow of the low ions, we see a lack of the intermediate velocity (70 to 80 km/s) infalling low ions otherwise found throughout the sky (Danly 1989).

In addition to the unusual kinematics of the gas in the region, the line of sight toward HD119608 also has unusual ionization characteristics. HD119608 is the only high latitude star to show absorption from the very highly ionized ion N V, an indicator of hot gas. The other widely studied highly ionized species, C IV and SI IV, are also present.

We carefully analyzed absorption data toward nine stars in the region, which are described in Table 1. An unusual velocity separation between highly ionized species and low ions appears in the absorption spectra toward HD119608 and two other stars, HD121968 and HD125924, within ten degrees of galactic latitude to HD119608. In summary, these observations suggest interesting flows of both hot and cold gas, which may be indicative of a galactic chimney. Observations in other regions of the galaxy reveal none of these characteristics.

Table 1: Star Data

Name	MK type	l	b	RA	Dec	z	V	Ref
HD117880	B9 IV/V	317	43	13 30 47.6	-18 15 24.9	0.33	9.1	1
HD119608	B1 Ib	320	43	13 41 48.2	-17 41 10.8	3.1	7.56	2
HD119786	A2 V2	322	45	13 42 53.2	-15 31 01.3	0.07	6.2	3
HD123883	B8/9 Iabp	328	41	14 07 48.5	-17 45 20.2	8.7	9.4	2
BD+2 2711	B2.5 V	330	62	13 40 44.0	+01 43 08	2.5	10.4	3-7
HD118246	B5 IIIe	322	55	13 33 66.7	-05 54 03.6	1.1	8.07	2
HD120086	B3 III	330	58	13 44 44 2	-2 11 40.1	0.85	7.89	8
HD125924	B2 IV	338	48	14 20 37.7	-8 01 15.9	2.4	9.68	8
HD121968	B1	334	56			4.3	10.31	8

References: (1) Albert 1983, (2) Albert et.al. 1992, (3) Tobin 1985, (4) Houk 1982 (5) Bidelman 1988, (6) Hill 1970, (7) Stetson 1985, (8) Danly 1989

Table 1 lists the stars included in the study. The top half were newly observed in this Trident project while the lower half of the stars were observed previously by Danly (1989) and Albert et al.(1992). MK type is the spectral classification of the star by the Morgan, Keenan and Kellman classification system. l and b are galactic longitude and galactic latitude in degrees. Stellar coordinates are right ascension (RA) in hours, minutes and seconds of time and declination (dec) in degrees, minutes and seconds. z is the height of the star above the galactic plane measured in kiloparsecs. V is the visual magnitude of the star.

The region of study extends from 306° to 332° galactic longitude and +34° to +64° galactic latitude. Galactic longitude (l) is measured starting with the position of the sun relative to the center of the galaxy at 0° and continuing around the disk counterclockwise from north to 360°. Galactic latitude (b) is measured going from 0° to 90° above the plane of the galaxy and 0° to -90° below the galactic plane. Figure 3 shows the halo stars in the region as they appear relative to one another on the sky measured in the celestial coordinates of right ascension and declination.

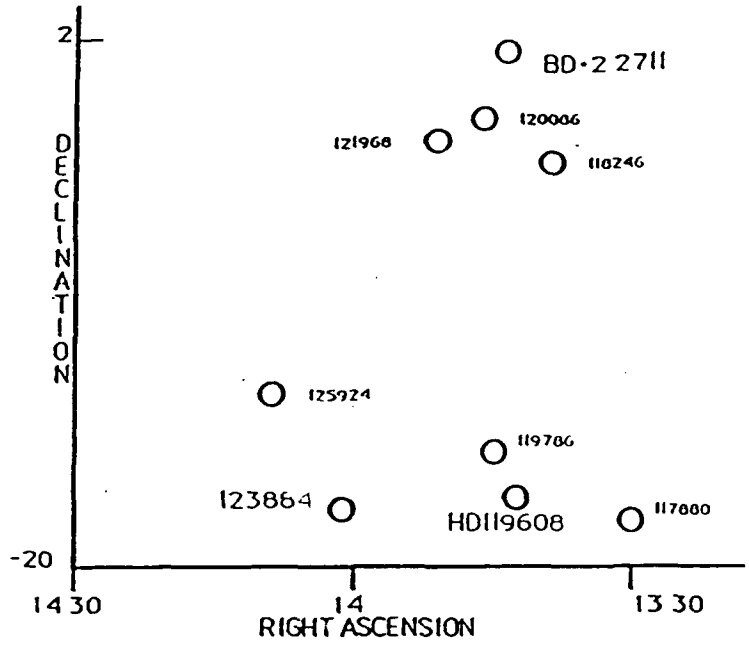

Figure 3: Background stars observed in the region plotted in coordinates of right ascension (hours and minutes) and declination (degrees) as they are seen in the sky in the constellation Virgo.

Figure 4 portrays the galaxy from a side view looking edge on to the disk as in the bottom part of the galaxy diagram in Figure 1, which shows the relative distances of the stars above the disk. In order to obtain interstellar absorption lines we must use a suitable star as a background source. Hot stars have an intense continuum and few absorption lines in the atmosphere of the star itself which might cause confusion with the interstellar lines. Also important in the selection of background stars is choosing distant stars of sufficient brightness to make observations. In order to establish constraints on the distance to the gas, we observed nearby foreground stars (HD119786 and HD 117880) and a star more distant than HD119608 (HD123884).

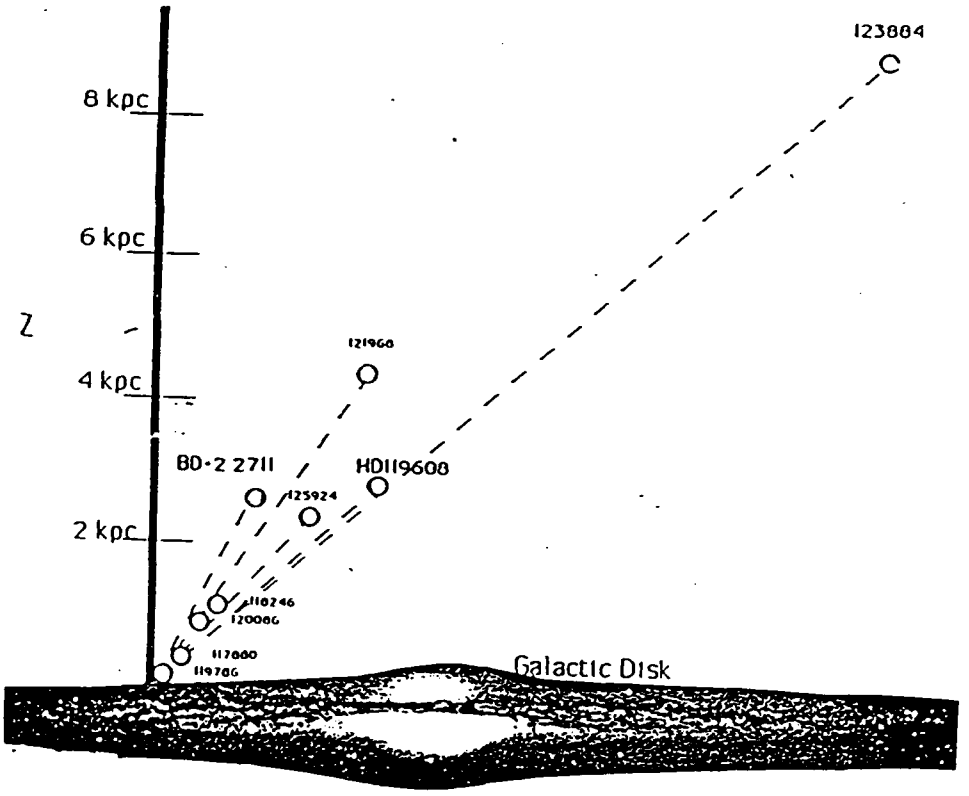

Figure 4: The stars in the region toward HD119608 in the halo of the galaxy with vertical height, z, in kiloparsecs above the plane. The angle of the stars above the plane is the galactic latitude. (Galactic disk is not to scale).

If an absorption feature is observed superimposed in the spectrum of a distant star but not toward a nearby star in the same direction, then we know that the gas of the feature must be located beyond the foreground star and in front of the distant star, unless the gas is extremely patchy and varies in the very small angle between the stars in the line of sight. In order to establish a vertical limit of the feature (how high the feature extends in galactic latitude) we observed the high latitude star BD+2 2711 at 62°.

The purpose of this investigation is to probe the region suspected to be a possible galactic chimney to determine spatial constraints (localize the unusual feature in space), obtain ionization and abundance information, and observe kinematic effects. The next three sections will discuss and analyze observations of the region in radio, optical and ultraviolet wavelengths. We then compare the results to the chimney model to support or refute the theory.

III Radio Observations and Analysis

Observations of neutral hydrogen emission give a spatial picture of the location of interstellar gas on the plane of the sky because emission can be observed in any direction, not just in lines of sight where background stars are available. The energy transition which results in the emission of a photon with a radio wavelength of 21 centimeters from a hydrogen atom occurs when the electron in the first orbital (n=1) and with angular momentum of 0 ($l = 0$) changes its spin orientation with respect to the spin of the proton in the nucleus (Figure 5).

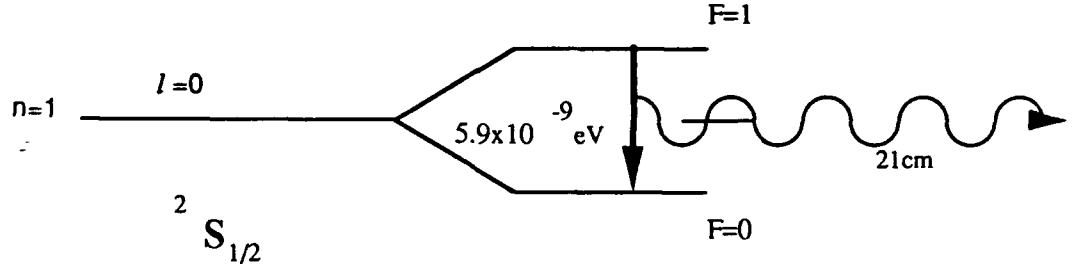

Figure 5: The energy level diagram of the ground state of neutral hydrogen.

The electron with its spin parallel to the proton (total spin quantum number (F) = electron spin + proton spin =1/2 + 1/2 = 1) "flips" to spin antiparallel (F = 1/2 - 1/2 = 0). The energy change is very small, only 5.9×10^{-9} eV, resulting in a very long wavelength of emission, 21 cm. This example of hyperfine structure (evidence of electron-nucleus spin interaction) occurs very rarely, with a probability of transition of one time in 10^7 years. Therefore, the H I hyperfine transition is considered "forbidden" in the relatively dense laboratory conditions on earth. In a dense gas, the spin flip is caused by collisions long before the low-probability spontaneous transition can occur.

In interstellar space, however, the average density of one atom/cm^3 is so low that the atoms remain in the excited state and the "forbidden" transition is common. Hydrogen makes up over 70 percent of all matter, and the enormous volume containing this most abundant element makes the spectral line very strong and easy to measure.

We constructed contour maps of the emission of neutral hydrogen over the northern galactic sky from the all sky survey done by Bell Labs (Stark 1992). The only marked region of outflow above the galactic plane was strongest at a velocity of 25 km/s and located in the region of our background stars. Figure 6 shows the contour map of the emission strength of the 25km/s outflowing gas over a polar view of the northern galactic sky.

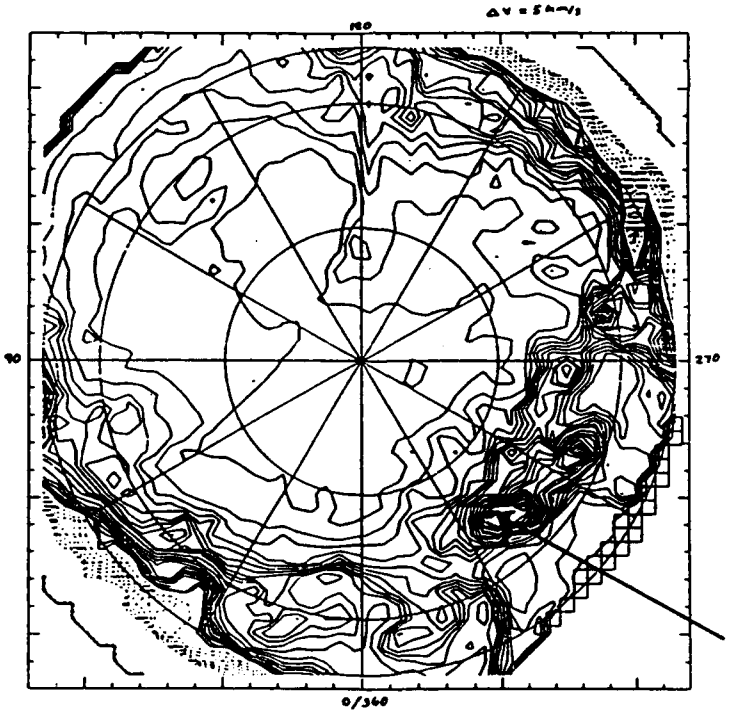

Figure 6: Bell Labs survey of the 21cm radio emission in the northern galactic sky mapped in contours indicating the 25 km/s outflow strength. The arrow indicates the outflow region where HD119608 is located.

Observations

The Bell Labs survey has the low spatial resolution of three degrees, so in order to fully explore the spatial characteristic of the outflow region at high resolution, we applied for observing time for this Trident project on the 140 foot radio telescope at the National Radio Astronomy Observatory (NRAO) in Green Bank, West Virginia, which is one of two radio observatories supported by the National Science Foundation. Completed in 1965, the instrument used for observation is the largest equatorial mount telescope in the world (Figure 7). NRAO granted us time on three occasions and we conducted observations on 1-2 April 1991, 10-12 August 1991, and 20-21 January 1992.

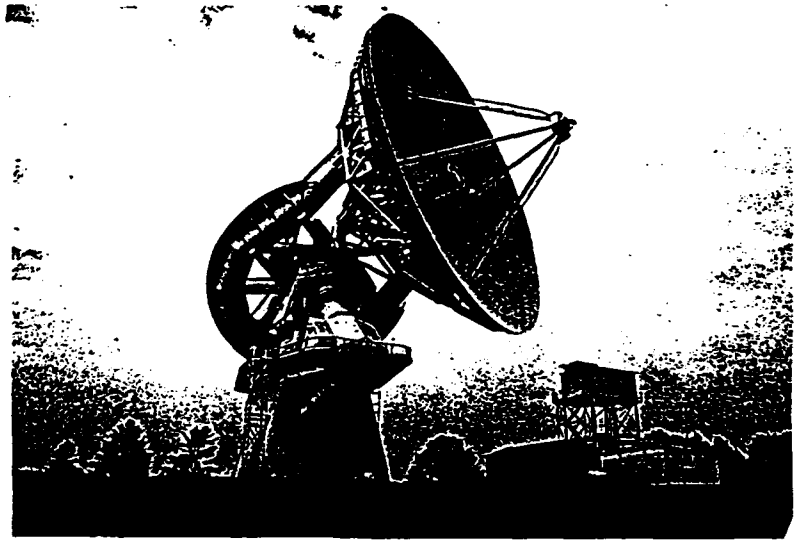

Figure 7: The 140 foot telescope of the National Radio Astronomy Observatory in Green Bank, West Virginia.

The telescope focuses the radio waves using a solid-surface, 140 foot diameter paraboloid at a focal ratio of 0.43 onto a receiver about the size of a refrigerator. Two antennas receive the signal at perpendicular polarizations. A complex system of cryogenics maintains the internal electrical system noise below the cosmic background radiation of 3 degrees Kelvin. The 150 ton telescope dish rotates on a single very large ball bearing which is kept constantly lubricated with a thin layer of oil on which the dish "floats". The telescope has a pointing accuracy and repeatability of 10 arcseconds (.003 degrees). Positioning parameters and information are written into a computer format which mimics the original punched cards first used at the telescope. The telescope operates automatically according to computer input, and a professional telescope operator monitors the computer and engineering systems and may enter commands manually. The observer directs the observations and can view raw spectra on a computer work station within minutes of the time they are taken.

We utilized our observing time to scan the region around HD119608, scanning along the horizontal direction across the sky in right ascension. Spectra were taken at a rate of 12 per minute with a 20 arcminute beam width. The right ascension "strips" with one spectrum every 10 arcminutes were taken at 30 arcminute intervals in the vertical direction of declination to construct a map of the radio spectra at the high spatial resolution of 20 arcminutes. The initial survey indicated a strong feature of outflowing gas at 25 km/s, and the subsequent observations extended the map to determine boundaries of the flow feature and to explore the higher latitudes around the star BD+2 2711.

As with all radio telescopes, the 140 foot has sidelobe radiation beams in addition to the main beam pattern. In halo gas in which the hydrogen emission is weak compared to that of the disk, accidental measurement of scattered signal picked up in the sidelobes can seriously degrade the data. Therefore, the program included observations toward each star to measure the stray radiation emitted into the telescope beam sidelobes and to compare these measurements with standard spectra. Comparisons to standard measurements indicate no significant stray radiation detections in our observations.

Radio Analysis

We observed over 3000 individual positions (times 2 polarizations gives over 6000 spectra) toward the region. The first step in analysis of the H I spectra is to determine a baseline which sets the background continuum to a value of zero. Almost the entire region has a very flat background radio continuum, so we used primarily a DC offset to simply move the base of the spectra to a zero flux value (Figure 8). The Unipops radio data analysis software package (written by Ronald Maddalena of NRAO) used to baseline the data allows baseline fits to polynomials in cases where the background is not flat. Parameters specified in the baselining procedure are the beginning and end velocities to include in the fit and the width of the regions to be averaged to determine the baseline offset. Figure 8 shows an example spectrum before and after baselining with a DC offset. The boxed regions indicate the points over which the average value for the offset was computed. The remainder of the data analysis was accomplished on the HI-IDL software package (written by K. D. Kuntz of the Space Telescope Science Institute). The baselined spectra are

transferred from the magnetic tape on which they are stored at the telescope in ASCII format into a disk file of a format readable by the HI-IDL software package.

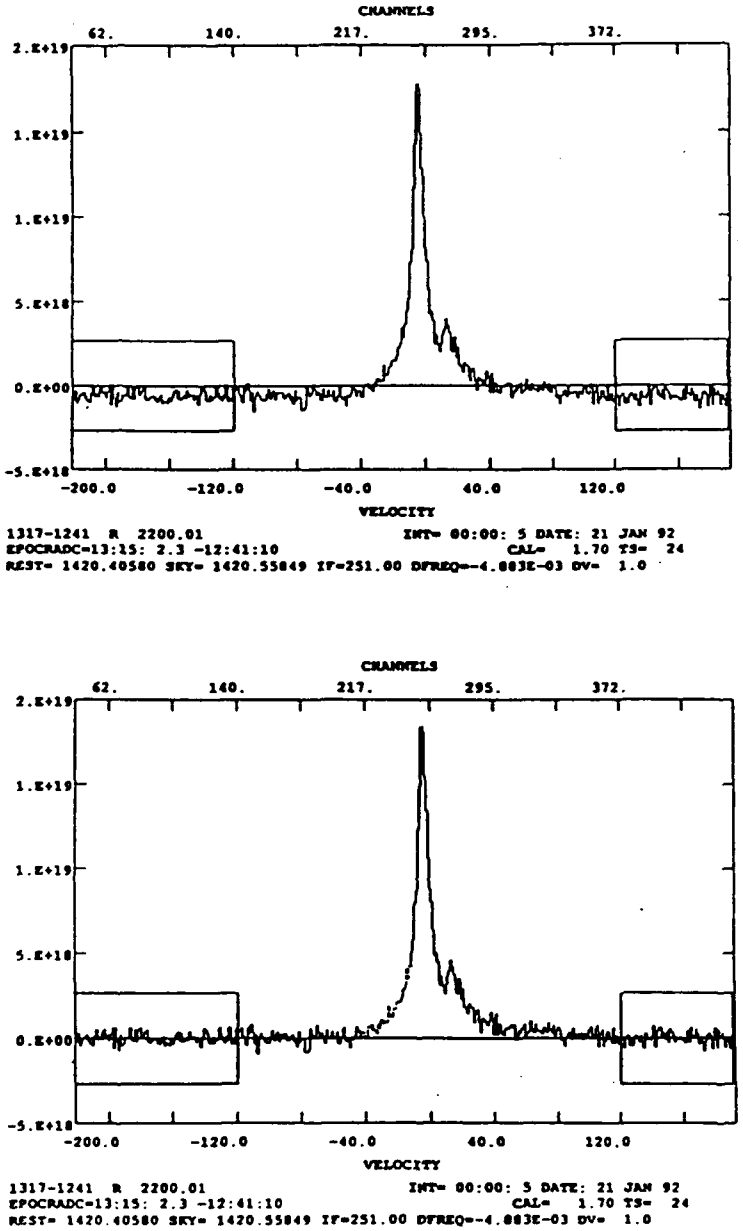

Figure 8: An example spectrum before baselining (at top) and after baselining the continuum (on bottom). The horizontal scale is velocity in km/s and the vertical scale is the actual number of neutral hydrogen atoms/cm^2 (column density).

To convert from measured antenna strength to brightness temperature (the standard unit of radio emission) and to correct for absorption in the atmosphere, we use the following relation (Williams 1972):

$$T_b = f\, T_a\, e^{\tau}$$

τ = 0.0101/cos (Zenith angle)

f = 1.0818 for antenna 1 (scan numbers ending in .01)

f = 1.0515 for antenna 2 (scan numbers ending in .02)

T_b is brightness temperature on the Berkeley scale

T_a is antenna strength (vertical axis of raw spectral plots)

The value of f is a function of the beam pattern of the particular telescope and antenna used and has been determined experimentally for the Green Bank 140 foot telescope. The atmospheric absorption is a small correction at radio wavelengths and depends on zenith angle (the angle from overhead to the horizon). The correction will be greater in observations at a large zenith angle than those high overhead since we are looking through more of the atmosphere at the horizon (Figure 9).

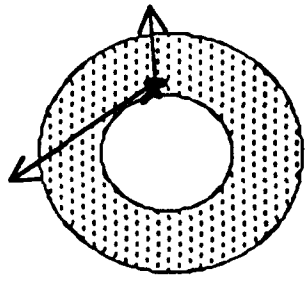

Figure 9: Qualitative demonstration that the path length of a wave through the atmosphere (indicated by the dotted region) is greater near the horizon.

We then divided the region into small areas or bins. The ideal lower limit of the bin size is the beam width of the telescope but the practical lower limit was the need to include more than one spectrum per bin. Fortunately, our beam size allowed an average of three spectra per bin (Figure 10). We divided the velocities into segments to look at the strength of the emission in a discrete velocity increment. Shown below on the left are the position of the spectra indicated by dots and on the right the bin grid overlap indicating the spectra in each spatial bin.

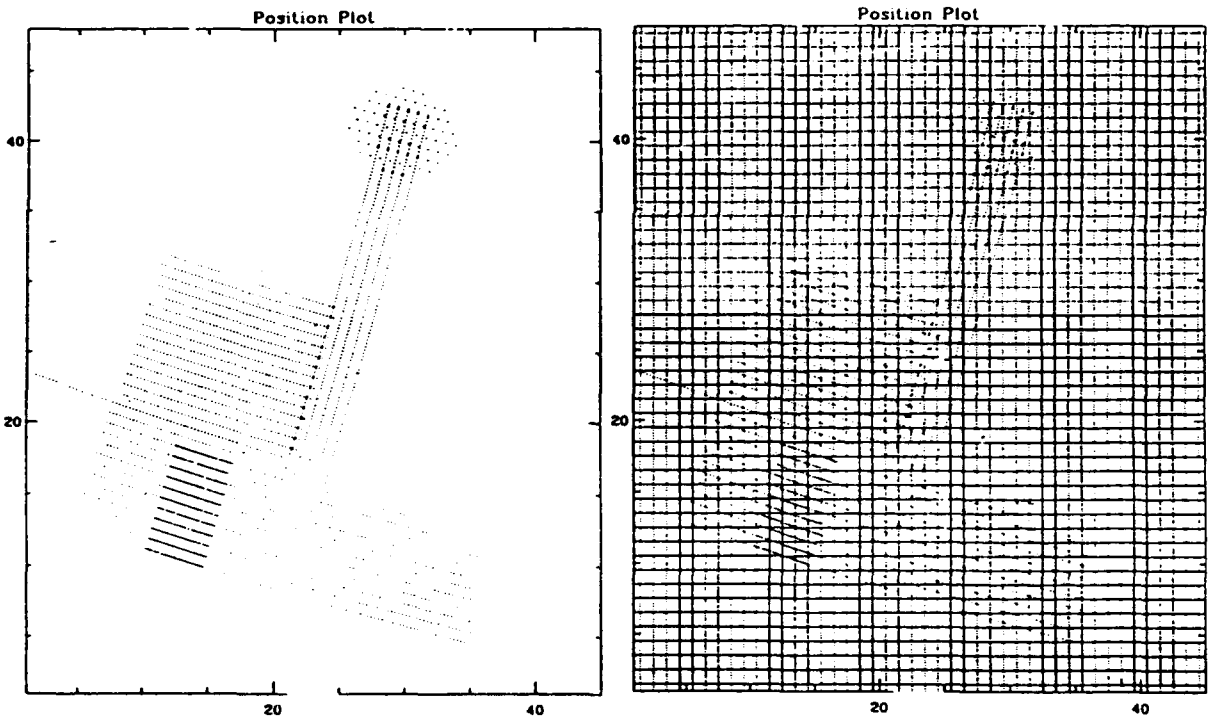

Figure 10: Left: The position of individual scans as dots. Right: The grid overlay showing the spectra in each spatial bin.

Using the two dimensional array called a channel map, which contains the values of the integral of the brightness temperature over the given velocity increment Δv and bin space x and y, we get column density (N) at each spatial bin:

$$N = 1.823 \times 10^{18} \times x \times y \times \int_{v}^{v+\Delta v} T(v)dv$$

The column density is the actual number of atoms along the line of sight producing the observed spectral feature. Contour maps of the column density in the observed region were constructed for each 5 km/s increment from -100 km/s to 100 km/s.

Of particular significance is the strong outflow apparent at the 25.5 km/s (Δ velocity of 2.5 km/s on either side) outflow map (Figure 11). Black indicates no observation was taken in the region or no gas was seen in that velocity range. The white square outlines the single bin space in the observed region containing no spectra. White is the lowest level of column density, which is at the lower limit of the signal to noise detection limit. The levels are filled in successively darker shades with each column density level as shown in the legend.

The position of several of the observed stars are shown on the contour diagram. The map shows the strongest outflow (darkest level) in the area of HD119608 with weak outflow on the lower longitude side at the right around the position of the star HD123884. At this velocity, the column density generally decreases as the latitude increases to the star BD+2 2711. Included in Appendix A are all of the velocity contour maps over the velocities from -100 km/s to +100 km/s. The contour levels are the same for all maps.

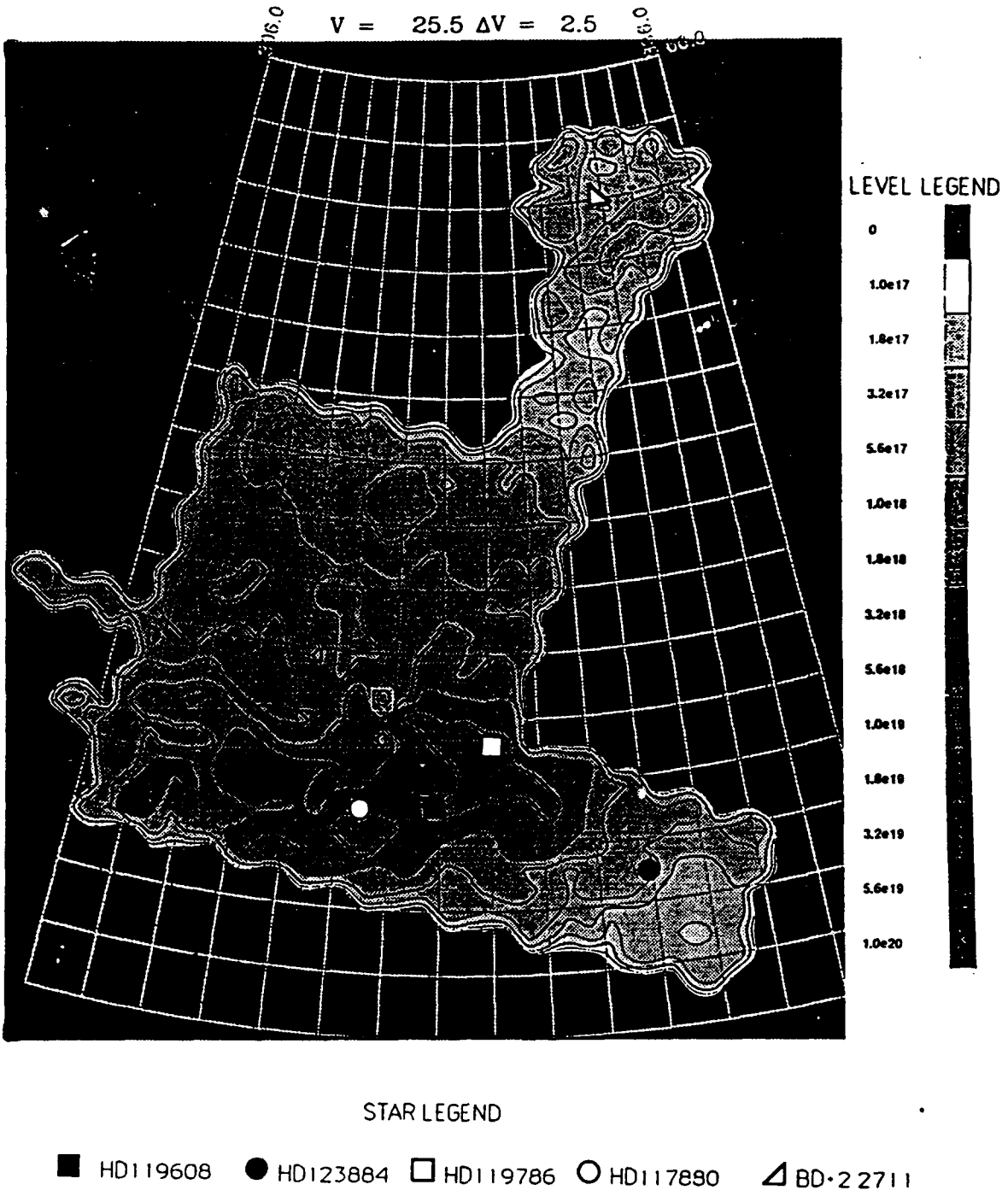

Figure 11: The contour map of neutral hydrogen emission strength at the strongest positive velocity feature at the velocity of 25 km/s.

Figure 12 shows the clean "on star" spectra toward each of the observed stars (Albert et al. 1992). The 25 km/s feature can be easily distinguished in the emission spectra toward the stars HD119608, HD117880 and HD119786. The 25 km/s emission is very weak toward HD123884 and relatively weak toward BD+2 2711.

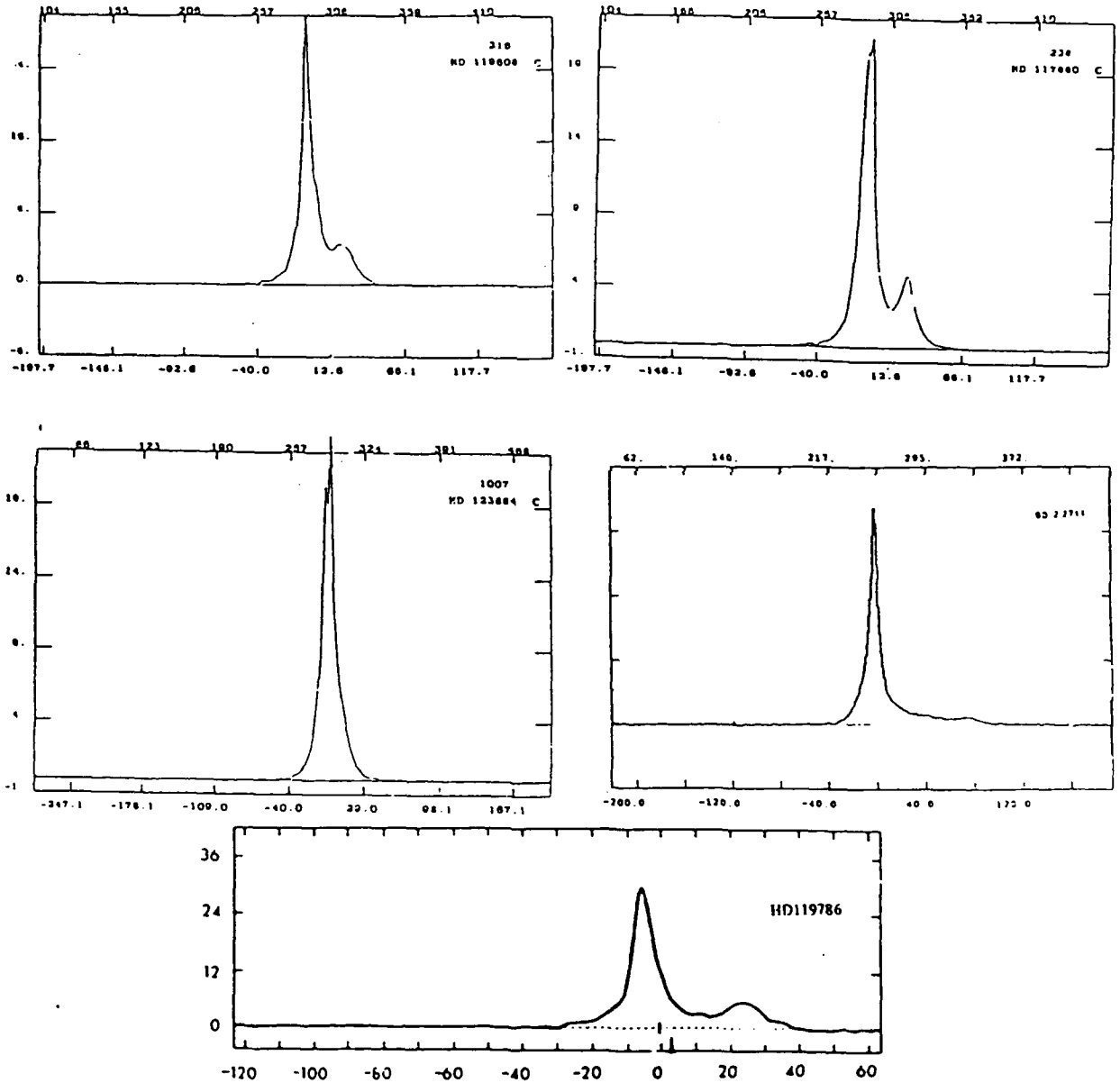

Figure 12: The individual neutral hydrogen emission spectra from the direction of HD119608, HD117880, HD123884, BD+2 2711, and HD119786. The spectra each cover slightly different ranges of velocity as shown on the horizontal scale in km/s. The vertical scale is brightness temperature.

IV OPTICAL OBSERVATIONS AND ANALYSIS

While the 21 cm neutral hydrogen emission gives a two dimensional map of the velocities of hydrogen gas in space, it does not tell us how far above the disk the interstellar gas clouds are located. In order to determine distance limits, we use very high velocity resolution optical absorption spectra. The K line of singly ionized calcium at 3933.633 Å toward HD119608, HD117880, HD118246, HD 119786, and HD123886 and the line of singly ionized titanium at 3383.761 Å toward the first four of these stars were observed in a large survey of halo gas by Albert and Blades (1992). The optical absorption observations were conducted using a charge coupled device (CCD) detector with the echelle grating of the coude spectrograph of the Canada France Hawaii Telescope on Mauna Kea, Hawaii. The resulting spectra achieved an average velocity resolution of 5 km/s. Figure 13 shows the singly ionized calcium (Ca II) line toward each of the stars and the line of singly ionized titanium (Ti II) toward HD119608.

The digitized spectra are shown as plots of intensity versus velocity. In most interstellar studies, velocity is measured with respect to the Local Standard of Rest (LSR), a reference frame defined by averaging the motions of nearby stars. As gas moves away from us out of the plane of the galaxy, its spectral lines are red shifted to longer wavelengths and positive LSR velocities. Infalling gas will show blue shifted absorption with shorter wavelengths and negative LSR velocities. The horizontal axis of the spectra is the velocity of this Doppler shift in km/s. The vertical axis of an absorption line shows the intensity of the detected light, with the background continuum starlight normalized to one. The line "drops" in intensity at velocities where the gas has absorbed some of the background light.

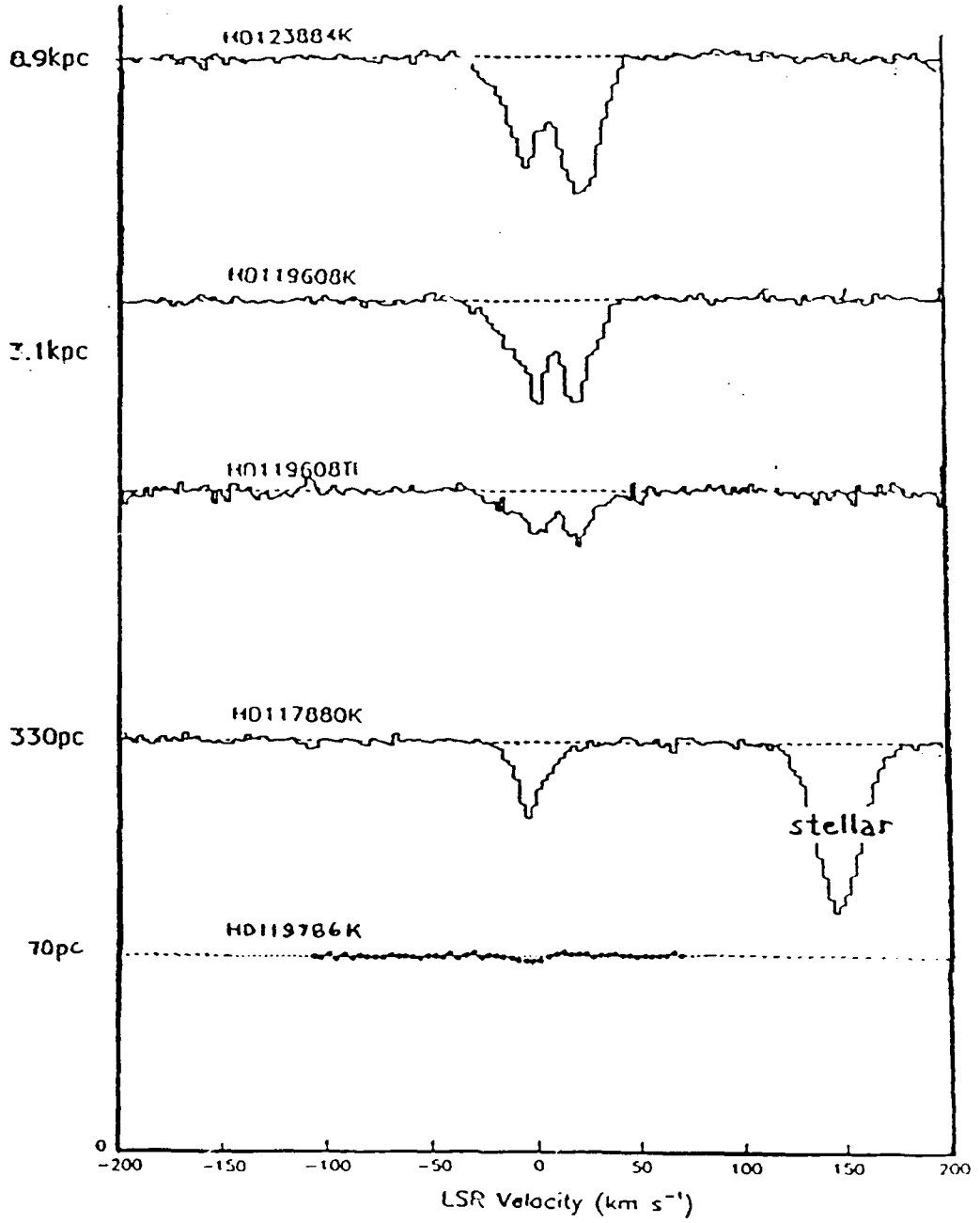

Figure 13: The optical absorption lines of singly ionized calcium towards stars at varying heights above the disk and the spectrum of singly ionized titanium toward HD119608.

Singly ionized calcium is one of the strongest and best studied of the optical interstellar species. Ti II is more difficult to observe, as detector sensitivities fall off considerably at this wavelength, so titanium can only be observed in the brightest stars.

Optical Analysis

Analysis of the absorption spectra gives us information about distance and ionization of the clouds. It is clear from the spectra shown in Figure 1 that very little gaseous calcium exists up to a distance of 70 pc above the galactic plane, and a weak zero velocity feature is located between 70 and 330 pc. A very interesting outflowing cloud centered at +25 km/s appears between 330 pc and 3.1 kpc, which is the distance to HD119608. It is also observed as a weak feature in the spectrum of Ca II toward a neighboring star, HD118246, at a height of 1.1 kpc above the galactic plane (Albert 1992). The 25 km/s feature becomes stronger in the spectrum of the more distant star HD123884, showing that more outflowing gas lies between HD119608 and HD123884.

The observed features in the spectra are actually the superposition of absorption from many clouds at varying distances and perhaps with varying physical conditions along the line of sight. To understand the properties of the different clouds that form an absorption line requires the detailed analysis of the line profile to separate individual clouds. Cloud modelling can only be done with high resolution data.

The modelling was accomplished using the profile fitting routine of the KDAF spectral data reduction software package written by K.D. Kuntz of the Space Telescope Science Institute. The routine takes as input a model of many clouds along the line of sight each specified by central cloud velocity, Doppler broadening (which depends on cloud temperature), and column density. The routine uses the cloud parameters to create the line profile of a given spectral line as it might be observed with a particular instrument. This simulated line

profile can be compared to the measured line profile. To construct a model, we varied the parameters to get the best possible fit with only one cloud, then two, etc., adding clouds until the modelled profile matched the observed profile to within the signal to noise limit of the data. The resulting models of HD119608 and HD123884 each contained eight clouds. The positions and Doppler widths of the clouds remained the same for both stars, but the column densities were increased for HD123884 to account for the greater distance of that star. The profile fitting technique gave us column densities of the calcium at the distances to each star and showed outflowing calcium clouds at velocities around 25 km/s, high above the plane of the galaxy.

To understand the physical conditions in each cloud, it is necessary to determine whether the hydrogen gas, which forms the bulk of the interstellar material, is neutral or ionized. Observations of Ca II determine neither the gaseous abundance of calcium nor the level of ionization in the cloud, since both Ca II and the unobservable Ca III may coexist in neutral or ionized hydrogen regions. Singly ionized titanium, however, is a unique tracer of neutral hydrogen due to the almost exact coincidence of the ionization potentials of Ti II and H I. A cloud observed in Ti II is almost certainly a neutral hydrogen region and the strength of the Ti II absorption line does reflect its true gaseous abundance. The Ti II line toward HD119608 matches well with the Ca II line and also shows the 25 km/s outflow feature indicating that both species are indeed in the same cloud as the neutral hydrogen. On the other hand, the neutral hydrogen spectrum observed in radio emission toward HD123884 (which shows the strongest outflow of Ca II) is surprisingly weak in the positive velocities. Although HD123884 is too faint to obtain Ti II spectra with current technology, the lack of H I indicates that the line of

sight toward HD123884 does not go through the neutral cloud itself but through the ionized outer edge. This is a very interesting and unique opportunity to probe the detailed inner and outer structure of an interstellar cloud.

Titanium and calcium also share the useful property of being refractory elements. Such elements can very easily condense out of the interstellar gas onto solid dust grains and are easily released back into the gas phase if the grains are destroyed by a passing shock front (Jenkins 1986). Absorption lines of Ca II and Ti II would therefore be enhanced in gas that had been shocked by a supernova remnant or had been propelled through high velocity flows such as a galactic fountain or chimney. The lines observed toward the stars HD119608 and HD123884 are strong compared to typical disk gas and are consistent with a chimney scenario.

V Ultraviolet Observations and Analysis

The optical observations were conducted with the most advanced ground based technology at high resolution which allows detailed analysis of individual velocity components in the absorption spectra. The high resolution is critical to the identification of the weak, narrow components of numerous clouds which are superimposed in a typical interstellar absorption line and to distinguish the lines of many different elements found in a very small range of wavelength. However, only a very limited number of ions absorb in the wavelengths visible to the human eye. Due to atomic structure, many more ions have strong resonance absorption lines in the ultraviolet band of the spectrum. Therefore, even though ultraviolet spectra (with average resolution of 25 km/s) cannot achieve the high resolution of optical

observations (5 km/s), the spectra in the ultraviolet wavelengths from 1190 to 2070 Å proved essential in providing ionization and abundance information. As part of this prohect, we applied to NASA in January of 1991 for use of satellite time, and were able to obtain spectra with the International Ultraviolet Explorer (IUE) satellite in three shifts from 26 to 28 June 1991. We observed HD123884 in two shifts and BD+2 2711 in the third shift from the ground station at the NASA Goddard Space Flight Center in Greenbelt, Maryland.

Launched in 1978, the IUE satellite orbits the earth in an elliptical geosynchronous orbit in which the craft is always visible from one of two ground stations, the Goddard Space Flight Center operated by NASA or the Villafranca Satellite Tracking Station near Madrid, Spain operated by the European Space Agency. Goddard controls the satellite during two eight hour shifts each day and VILSPA operates the third shift.

Two large solar panels power the spacecraft with a backup battery for periods when the satellite travels through the earth's shadow (Figure 14). The on-board computer controls telescope pointing, execution of movements, and exposure time. The satellite has three axis stability (roll, pitch, and yaw) and a nominal pointing accuracy of one arcsecond. Attitude control is accomplished using the two remaining operable gyroscopes of the original six, together with the Fine Sun Sensor which detects the position of the sun (Sonneborn et al. 1987). Reaction wheels are used to store angular momentum and accomplish spacecraft rotation. Therefore, after a movement of the telescope into position (called a slew), and before observations are made, the wheels often must be "unloaded", using small hydrozene jets, to establish proper momentum.

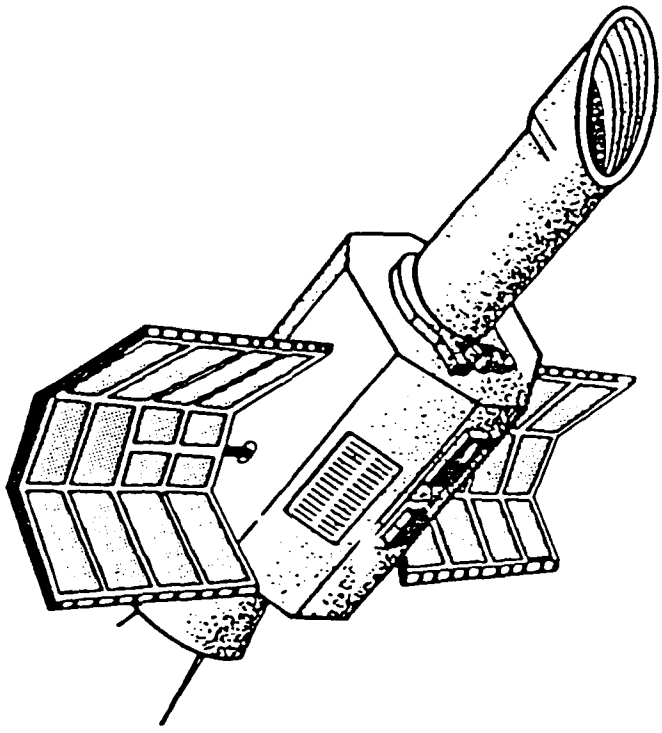

Figure 14: The International Ultraviolet Explorer Satellite operated by NASA and ESA.

During observations, a telescope operator and resident astronomer control the satellite and provide technical assistance, with directions from the guest observers. Operations Control Center personnel monitor all of the engineering functions of the satellite in a building nearby the Telescope Operations Center. The ground station transmits commands to the satellite at VHF (Very High Frequencies), while the satellite in turn relays information at a rate of 20 kilobytes/sec in the S-band frequencies. An 18 meter antenna at the International Ultraviolet Explorer (IUE) tracking station on Wallops Island, Virginia, receives the information from the satellite and forwards the data to Goddard via a communications satellite.

The IUE spacecraft has four cameras and two spectrographs. The two spectrographs, one for short and the other for long ultraviolet wavelengths, and each has a primary and a redundant camera. We made each of our observations using the SWP (Short Wavelength Prime) camera. The camera

electronically counts the number of photons in each wavelength registered in photomultiplier tubes. Over the exposure, the image is integrated in the SEC Vidicon section of the camera. The camera retains its image until the information is read down to the tracking station using a raster scan of 768x768 pixels. The video signal is digitized into 256 discrete levels (0 to 255 Data Numbers (DN)) by an eight bit analogue to digital converter. Real time transmission occurs to the ground station and a residual image remains on the camera until after a PREP is executed. A PREP consists of exposing the image with a tungsten flood lamp to get a reproducible electronic pedestal of 15 to 40 DN. To check the camera, a reading is then taken with the defocused beam and the exposure and reading are repeated. The PREP procedure basically exposes the image to a constant starting background to get rid of the leftover image from the previous observation. During observations, incoming light is focused onto an echelle spectrograph which separates the light into its various wavelengths giving a series of strips called orders. Photons at each wavelength then register in photomultiplier tubes. Careful monitoring of background radiation is required throughout an observation to avoid overexposing and damaging the instrument.

Ultraviolet Observations

To conduct an observation toward a star, we make a finding chart from the Palomar Sky Survey prints to identify the star in the image from the satellite's Fine Error Sensor (FES). The FES uses a photocathode that has a peak response in the visible wavelengths to provide a television image of the field of view. When the target has been properly identified, the exposure is begun. At the end of the exposure the image is read down and can be viewed in the

form of a photowrite (Figure 15). The digital spectrum is stored from the computer onto magnetic tape for future analysis. Two observations were taken of HD123884: a 420 minute exposure on 26 June 1991 recorded in the file "SWP41921hlg" and a 430 minute exposure on 28 June 1991 in "SWP41944hlg". One 320 minute exposure of BD+2 2711 is recorded in "SWP41932hlg". All of the observations made on IUE become public record in archives a year after the observation. HD119608 was observed in 1979 and we used the archived spectra toward this star in addition to our own observations of HD123884 and BD+2 2711 for our ultraviolet analysis.

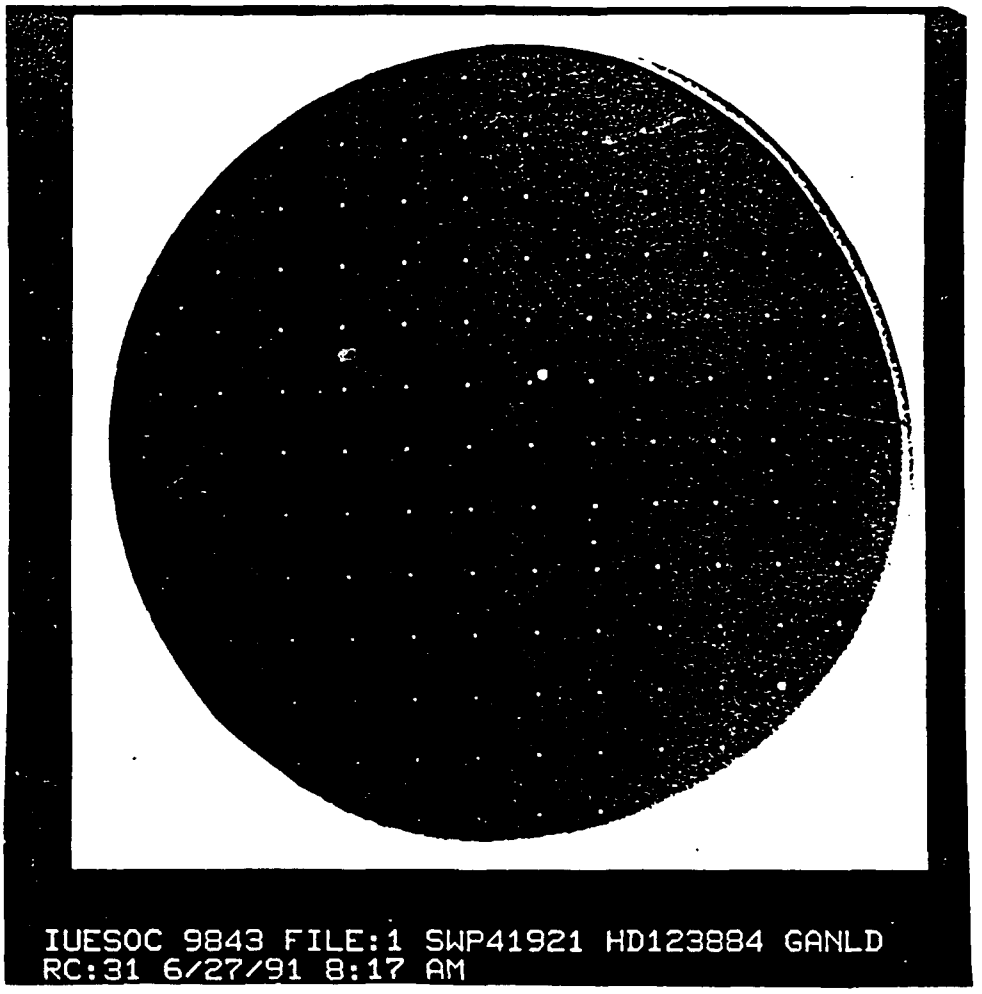

Figure 15: A photowrite, which is a photographic representation of the observed spectrum of the star HD123884. Each strip is an order. Evenly spaced white marks are reseaux (alignment marks). Black spots are cosmic ray hits.

Ultraviolet Analysis

The spectral files from the magnetic tape of the observing run were transferred onto disk files on the "Sol" computer system at The Space Telescope Science Institute where all of the analysis of the ultraviolet spectra was accomplished using the KDAF spectral data reduction software package. The analysis of the ultraviolet spectra requires a series of corrections and procedures in order to obtain each individual interstellar absorption line for study. We extracted each spectral line of interest as specified in an atomic line data file [See Appendix B: Atomic Line Data File] and over a given velocity range (-1500 to 1500 km/s).

Several types of corrections to the data are necessary before actual line strength measurements and profile modeling can be undertaken. Corrections include: reseaux corrections, cosmic ray hit corrections, coaddition of multiple spectra of a common star, correction to the flux for scattered light between adjacent orders, and the fitting of a background and stellar continuum. Reseaux are markings placed in the optics of the telescope in order to enable the geometric correction of the spectra. by determining the distortion of the optics due to temperature changes. The geometric correction is done automatically at the IUE ground station as the spectra are reduced from the satellite readout. The reseaux markings, however, block sections of the spectra (Figure 16) and are also easily seen as the evenly spaced white spots on the photowrite. This "bad" data is flagged with a dotted line so that it is not included in the analysis of the absorption line.

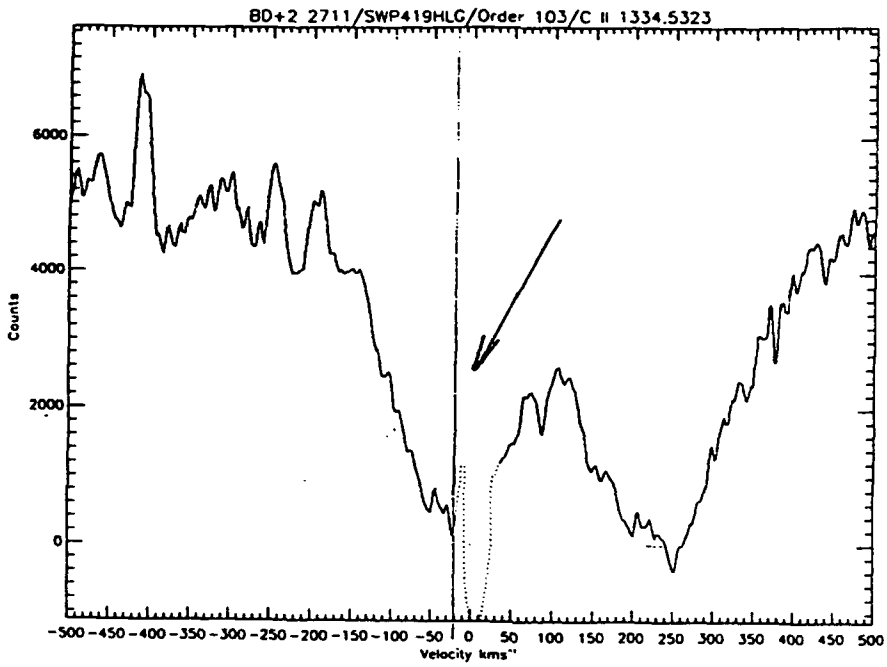

Figure 16: A reseaux mark (dotted line segment) in the optics obscured part of the spectrum of C II at 1334 Angstroms.

Occasionally the "bad" data quality flag extends to segments of the spectra which are in fact good data as can be determined from comparison with other spectra toward the same star or through simple visual inspection. (Figure 17). The improper data quality flags must be changed in the spectral line file.

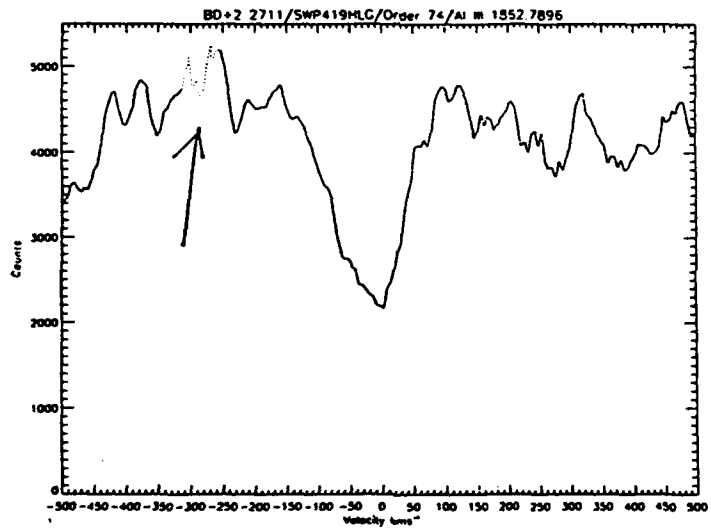

Figure 17: An improperly flagged region (shown as the dotted segment) of the Al III line at 1862 Angstroms which is actually good data.

Conversely, regions of a line where a cosmic ray has hit the detector, resulting in a noise spike, have to be reflagged as bad data (Figure 18) and these ray hits appear as very black spots on the photowrite image.

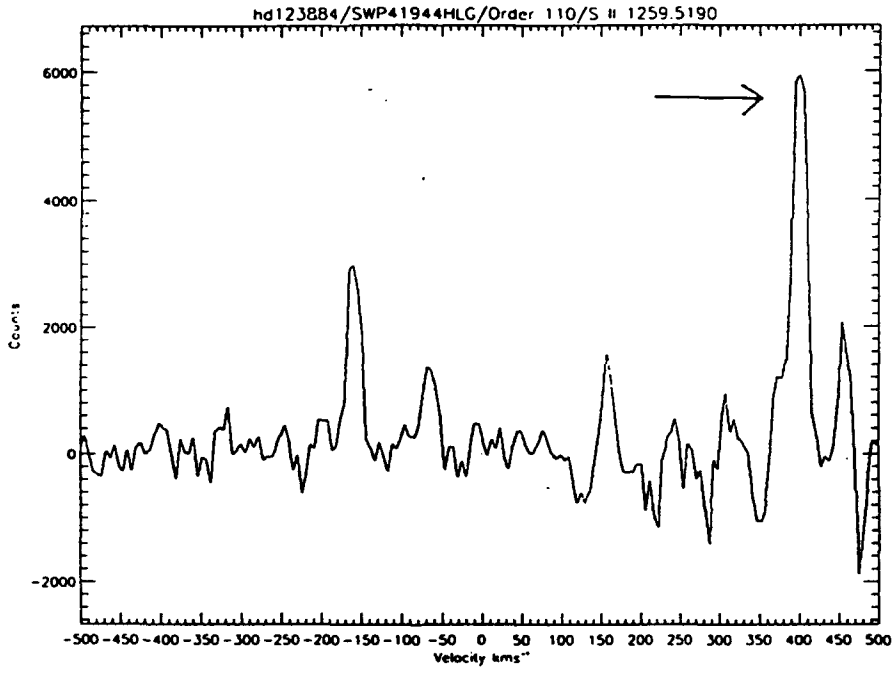

Figure 18: The enormous flux spike found at the location of a cosmic ray hit on the detector.

Coaddition (the averaging of the flux values for the two lines) of multiple images of the same star has several advantages. The two observations of HD123884, for instance, were taken with an intentional velocity offset so that the rescaux marks would not obscure the same part of the spectrum in both observations. Through coaddition, the signal to noise ratio improves by a factor of $\sqrt{2}$ and most of the spectrum will have "good" data quality flags. In order to coadd spectra, the velocity offset must be corrected so that both spectral lines are centered at the proper velocity.

The IUE spectrum consists of many orders which overlap slightly in wavelength at the ends of adjacent orders. The proximity of the orders, especially in the shorter wavelength region, causes the scattering of light from one order onto the order next to it. The scattered light gives artificially high flux for which the software compensates by setting the zero flux level too high. The scattered light correction is determined by looking at known saturated lines which should have zero flux at their bottom and shifting the zero flux point to this level. We apply the correction to all of the lines in that order and interpolate for orders containing no saturated lines. The scattered light correction introduces uncertainty in the data because saturated lines have noise and are not perfectly flat at the zero flux, so the level must be estimated through visual inspection or through taking an average of the flux over the "flat" region. Many orders have no saturated lines yet are obviously affected by scattered light and must be corrected with the best approximation (Figure 19).

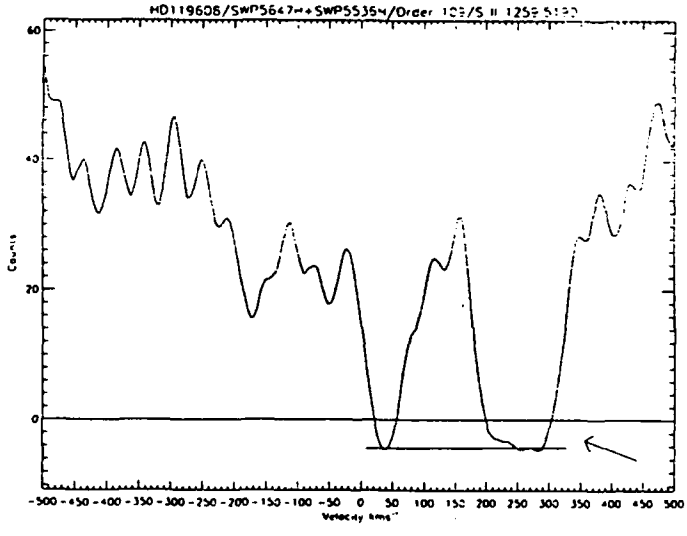

Figure 19 : An example of a line in an order with scattered light. The 1260 Angstrom Si II line is saturated, and the bottom of the lines serves as a reference for the flux correction.

Before a spectrum can be analyzed for interstellar features, the background continuum of light from the star must be fit to the spectral line. The spectrum is then normalized by the background so that the light from the star has a flux value of 1 and regions where light has been absorbed by interstellar gas have values less than 1, with 0 being the maximum absorption for saturated lines in which all of the light at a given wavelength has been absorbed (Figure 20).

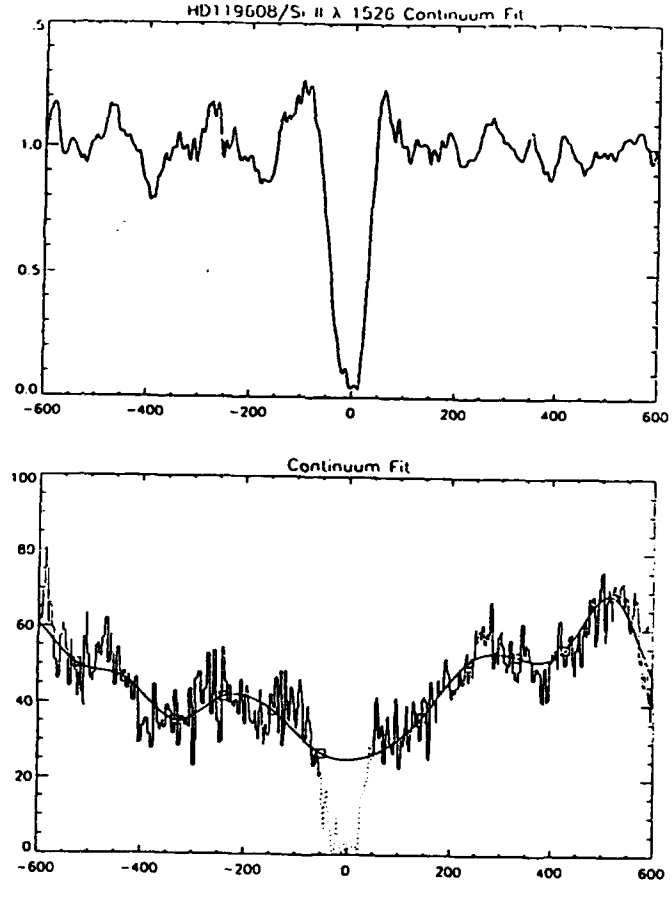

Figure 20: The continuum fit for the Si II 1526 line in HD119608 and the normalized spectrum. The boxes show the locations of cubic spline and the dotted line indicates the region excluded from the fit.

The procedure to set the continuum fit takes a given number of cubic splines and fits a continuum based on entered parameters which are: velocity range of fit, number of points over which to average for each spline, number of cubic splines to be calculated for the fit, regions of the line to be excluded from calculations, the number of iterations of the fit, and whether the splines are calculated at evenly spaced intervals or include the edges of excluded regions. For any given spectrum, there can be many possible fits to the continuum. In regions where the background continuum is relatively even, a fit is simple and the uncertainty introduced by the fit may be only a few percent. On the other hand, in regions where the stellar profile shows absorption from the atmosphere of the star, a unique fit is difficult or impossible, introducing considerable uncertainty in the continuum fit and the normalized spectral line. Results of the uncertainty include systematic errors in column density caused by an offset or incorrect central velocity caused by an incorrect slope. The distinction between the stellar and the interstellar absorption is a complicated question worthy of a separate section of discussion.

Stellar Ultraviolet Analysis

The background stars observed for this investigation in the ultraviolet were hot distant stars ranging in spectral type from B1 to B8/9. With surface temperatures from 10,000 to 25,000 Kelvin, these stars emit strong ultraviolet radiation making them excellent background sources for the study of interstellar gas, and are luminous enough to be observed at long distances. One difficulty present in the study of interstellar absorption lines, however, is that the atmospheres of the stars themselves also absorb certain wavelengths in the ultraviolet. Accurate analysis of the abundances of ions in interstellar

lines requires that no contamination from the star's own ions be included in the interstellar calculations. At this time, work is in progress to establish standard ultraviolet classifications of spectral type (Rountree and Sonneborn 1991) similar to the standards which have been established in the optical portion of the spectrum (Morgan et al. 1943). Some of the spectral types have been well observed and have been designated ultraviolet standard stars, especially those B type stars of average luminosity. Other less well observed superluminous type stars have yet to be set to definite standards. When standards are available, one can compare the standard star of a given spectral type to an observed star of the same type and the stellar lines should be the same. Since the standard spectra should be taken of nearby stars with virtually no interstellar lines, the interstellar absorption lines of an observed star would be obvious in comparison with the standard.

The problem is, in fact, more complex as the shape of stellar absorption lines depends on many different factors of the star's dynamics. The rotation of the star broadens the lines and generally makes them symmetrical. The velocity of the star toward or away from us causes a Doppler shift of all of the stellar lines by the same amount corresponding to the star's radial velocity. The amount of broadening and the shape of stellar lines depends on where in the atmosphere the ions are found; the ions at the outer edges of the star's atmosphere tend to give the broadest lines as this gas rotates the fastest. However, spectra of species in the outer atmospheres of some stars are subject to strange shapes caused by the asymmetric outflow of particles from some stars which is known as stellar wind.

Fortunately, the strong stellar lines in the stars we observed were very broad and sloping compared to the narrower interstellar lines. Strong stellar

Silicon III lines were observed in the spectra of all three stars. If there is interstellar Si III, its absorption spectrum is completely dominated by the stellar line. Excited fine structure Si II lines were also seen which have the same shape as the stellar Si III and look very different from the ground state Si II interstellar absorption (Figure 21). We know that the excited fine structure must be stellar because the density and pressure of gas in interstellar space would not be enough to produce these lines at a detectable strength; they could only be formed in a star.

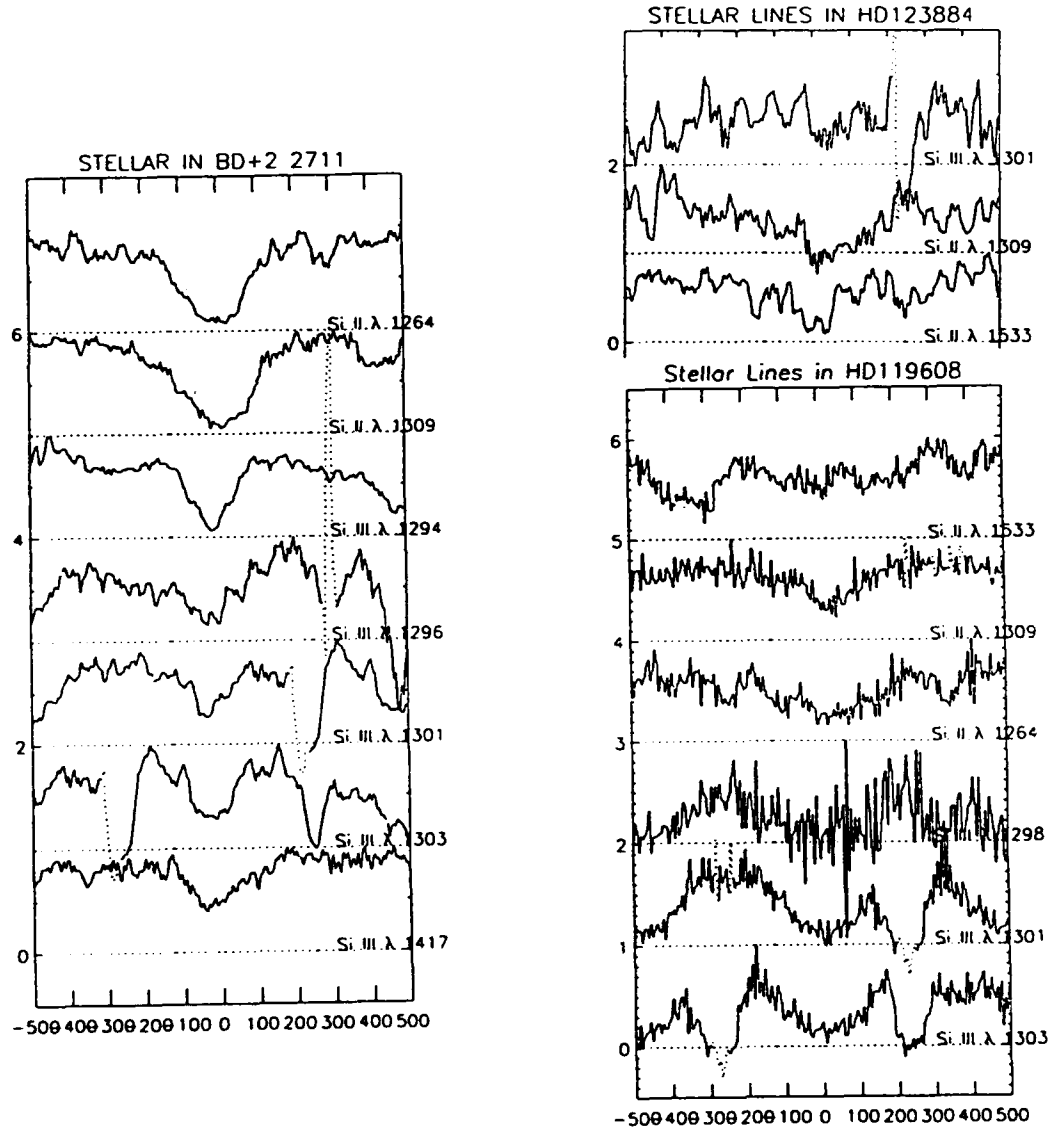

Figure 21 : Stellar Si III and Si II absorption lines (which have not been normalized since the stellar light is by definition the background).

In many cases, an obvious, narrow interstellar absorption line protrudes from the bottom of a broad, sloping stellar absorption line. The Carbon II lines at 1334 and 1335 A in HD119608 and the Aluminum III lines at 1854 and 1862 A in HD123884 are the most notable examples (Figure 22).

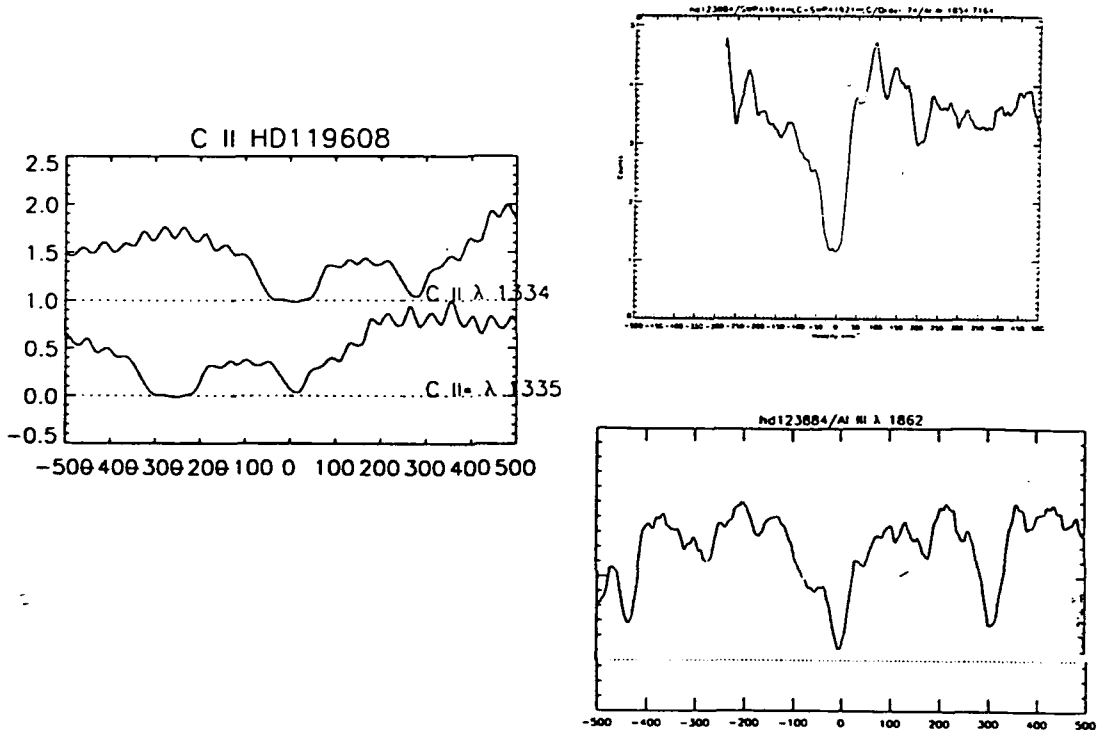

Figure 22: The unnormalized absorption lines of C II in HD119608 and Al III in HD123884 showing distinguishable stellar and interstellar components.

The most difficult lines to distinguish are those in which stellar and interstellar components both contribute significantly to the line. There is almost certainly interstellar Al III toward HD119608 and BD+2 2711 as well as Si IV toward BD+2 2711, yet we could only set limits on the interstellar abundances because we could not distinguish the stellar and interstellar components. Also, weak lines without a clearly stellar or clearly interstellar shape have generally not been as well studied as the strong lines that distinguish one spectral type from another. But, without particular

characteristics of the physical properties associated with the line, we cannot absolutely call such lines interstellar. For example, weak absorption lines with a very small but symmetric and sloping shape are seen at the positions of 2063, 2027, and 2022 A (which are the locations of excited fine structure Cobalt II lines) that should not be seen in the pressure and density regimes of halo gas and could therefore be small, weak, stellar lines. A more flat bottomed ground state Co II line appears at 2058 A which could be stellar, interstellar, or both: it is not possible to determine at this time with the low velocity resolution of the data. Higher resolution spectra from the Hubble Space Telescope's ultraviolet spectrograph may help answer some of these questions in the future. Also, one project that might be extremely useful for both astronomers studying the stars and those studying the interstellar gas would be a large scale study of the characteristics of the respective line types to establish a standard model of the stellar and interstellar lines. Their respective contributions to a given spectrum could then be systematically identified and separated.

Analysis of the Interstellar Absorption Lines

We made the necessary corrections and conducted preliminary analysis for a number of the clear interstellar absorption lines of neutral, singly ionized and highly ionized gas. Figure 23 shows the strongest and most easily detected species in each star. Because of the faintness of the distant star HD123884, two full night exposures, which were then coadded, are still underexposed and too noisy for accurate analysis in the shorter wavelengths of the ultraviolet spectrum. The long wavelength portion of the spectrum,

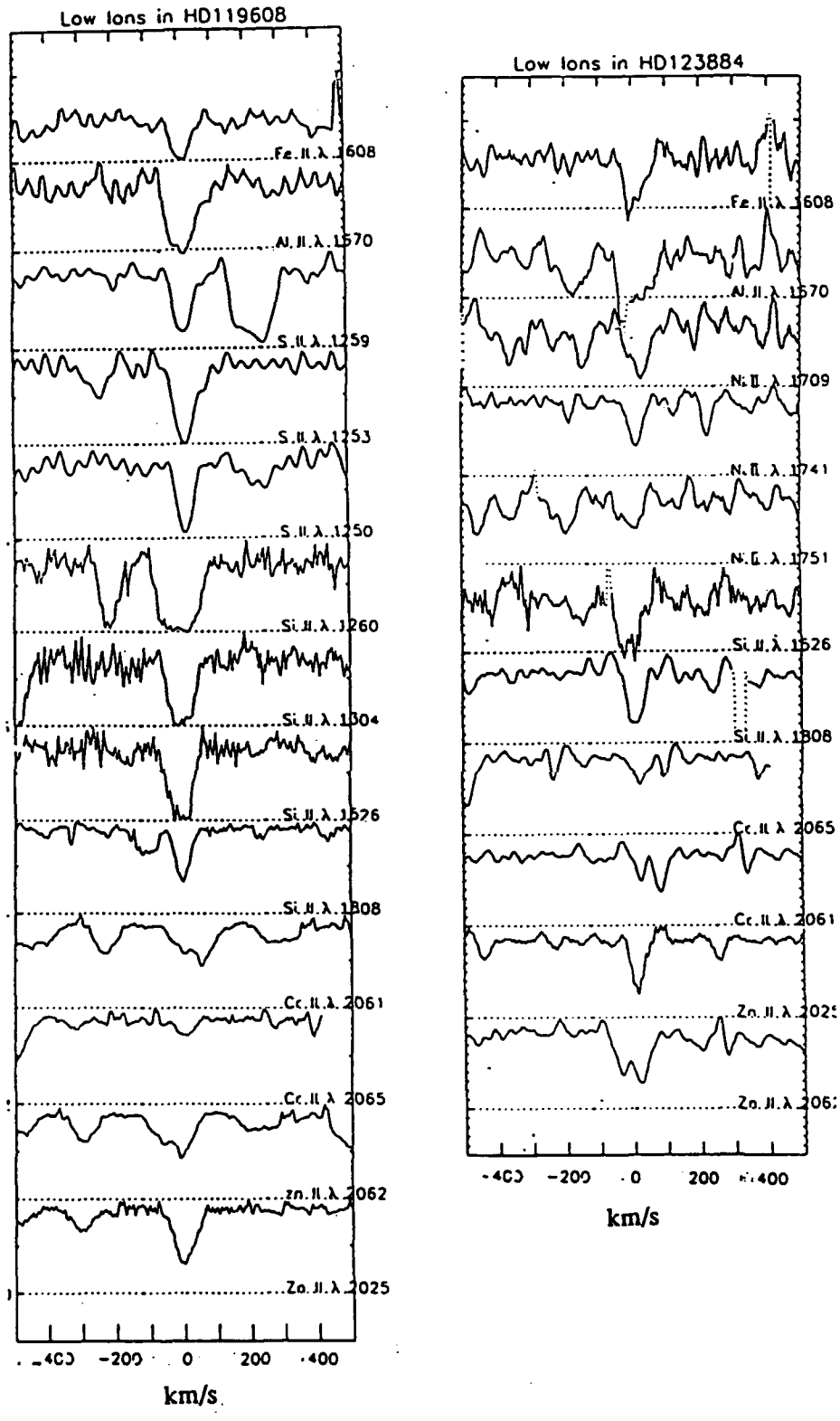

Figure 23: The strong ultraviolet absorption lines toward HD119608, HD123884, and BD+2 2711.

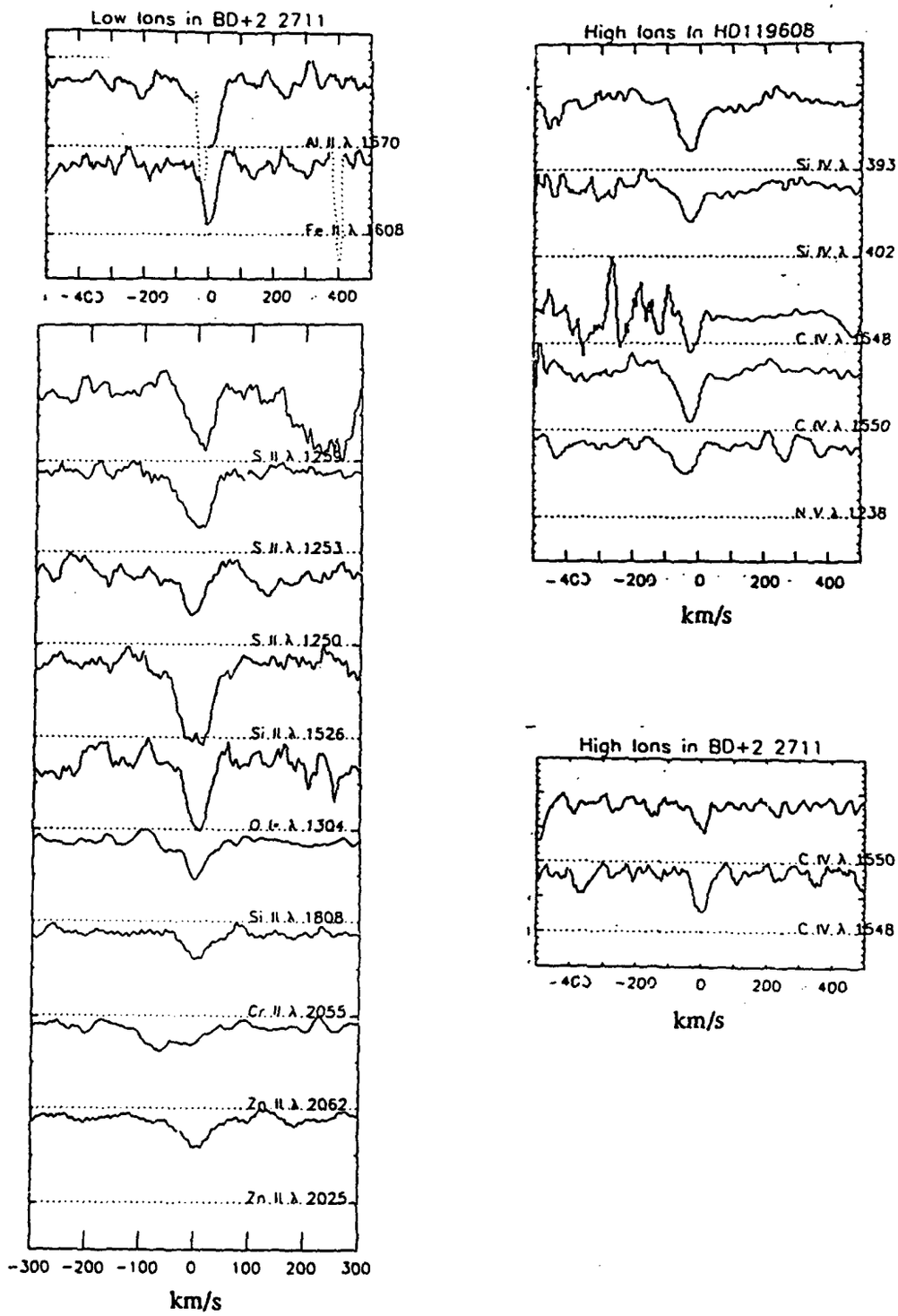

Figure 23 continued.

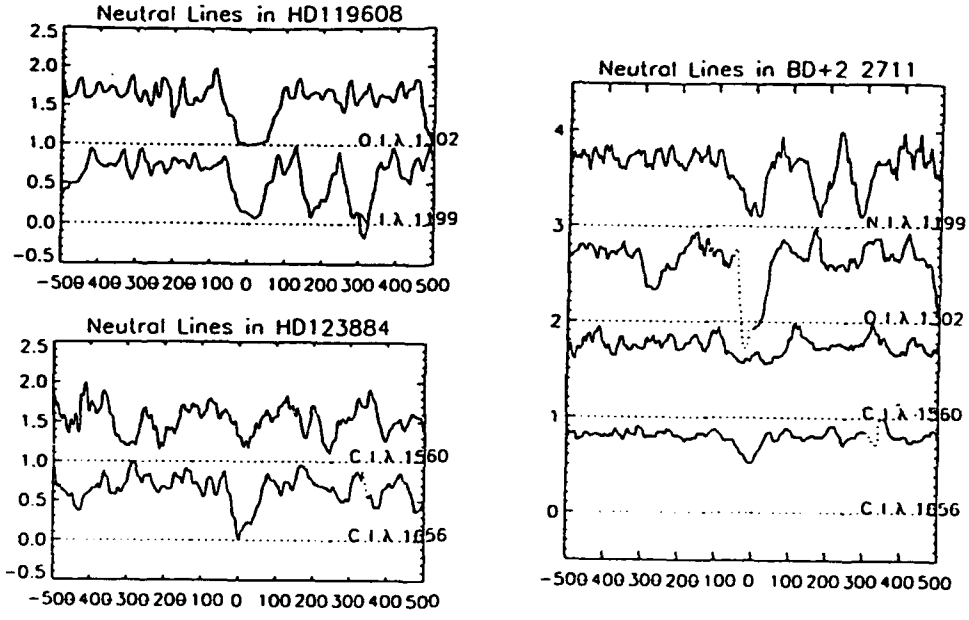

Figure 23 continued.

however, is well exposed and has provided important information about this line of sight. The original spectra of HD119608 from the archives had been extracted from the raw satellite data at Goddard Space Center when older software systems were in use. At our request, NASA re-extracted the spectra of HD119608 with the modern technique to make its resolution comparable to our other observed data. Upon receipt of the re-extracted spectra in April 1992, we reanalyzed most of the lines toward HD119608 at the improved resolution.

Ultraviolet Interstellar Analysis with the Curve of Growth

Once the spectra have been corrected and the continua have been fit and normalized, a curve of growth fitting technique is used to determine the abundances of the various ions. The first step in the process is to measure the area of the absorption line. Since the vertical height of the line is normalized to a background of one, the area measured has units of velocity which are

then converted to wavelength by scaling the value by the factor (λ / c) where λ is the wavelength of the line in Angstroms and c is the speed of light in km/s. The resulting value is called the *equivalent width.* The information which we want to know, however, is not the equivalent width, which is a measure of line strength, but the actual abundance of the gas in number of atoms, or *column density.* The relationship between the equivalent width and the column density is called the *curve of growth.* In general, the observed strength of a line increases as the column density "grows". For weak lines, the strength of the line is directly proportional to the column density. As absorption lines become saturated (all of the light is absorbed in a region), the curve becomes nearly flat and a large change in the number of atoms will result in very little change in the line strength. Eventually, if a line is extremely saturated, then the natural Doppler broadening caused by the average kinetic motions of atoms in the gas will cause the formation of "wings" or extended regions of the absorption line. The damping wings increase in area by a factor of the square root of the column density. We used the Macintosh Excel and Cricketgraph spreadsheet programs to plot theoretical curves of growth for different cloud temperatures, or Doppler broadening (b). Appendix C contains a more detailed mathematical description of the theoretical curves of growth. The theoretical curves are plots of the log of the equivalent width divided by the wavelength versus the log of the column density multiplied by the wavelength and the oscillator strength (a measure of the probability of an atomic transition). However, observed data is plotted as the log of equivalent width divided by the wavelength versus the log of the wavelength times the oscillator strength. The horizontal shift required to fit

the observed set of points for each ion to the theoretical curve of growth is then the log of the column density of that ion (Figure 24).

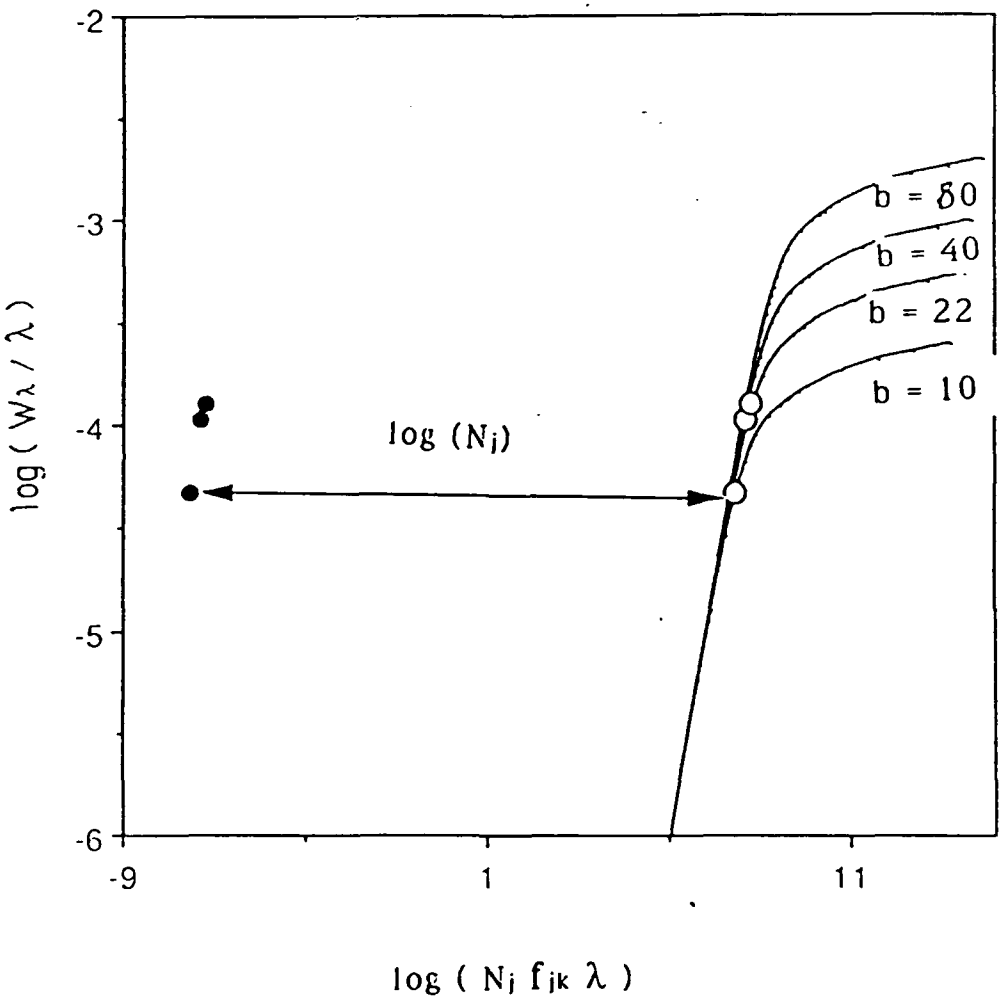

Figure 24: Theoretical curves of growth at different cloud temperatures, or Doppler broadening (b). The dark plotted points are the observed equivalent widths of the line of S II toward BD+2 2711. The shift of the data to the theoretical curve equals log (column density (N)).

This curve of growth technique gives the total column density of each fitted ion along the line of sight toward each of the stars observed in the ultraviolet. Appendix C also includes all of the fitted curves of growth.

Table 2: Column Densities by Curve of Growth Fit

Ion	BD +2 2711	HD119608	HD123884
Si II	3.55 E 14	1.00 E 15	2.00 E 15
S II	1.00 E 15	5.01 E 15	
Zn II	3.55 E 12	1.78 E 13	2.00 E 13
Cr II	1.26 E 13	5.01 E 13	3.98 E 13
Ni II	6.31 E 13		
C IV	6.31 E 13	8.91 E 13	
Si IV		2.29 E 13	
N V		5.37 E 13	

The total column density is the number of absorbing atoms along the line of sight in units of number of atoms/cm^2. The main source of uncertainty of the column density is the uncertainty of equivalent width typically 20 to 30%.

The principal experimental uncertainties in the column densities lie in the uncertainty of the equivalent width caused primarily by the uncertainty of the continuum fit which can cause about 20% variation in the measured equivalent width of strong lines. The uncertainty of column density is proportional to the uncertainty in equivalent width. In addition, there is some uncertainty in the best fit of the curve of growth, particularly with species in the "flat", or saturated portion of the curve. To help minimize uncertainty, with the exception of the single N V line, we only fit ions that have multiple absorption lines. The average uncertainty in fitting a set of points is much less than that of a single data value.

Spectral Analysis with Profile Fitting

The curve of growth fitting technique gives the overall column density of each ion, along the line of sight, but to determine the column density of each cloud component by velocity, we again used a profile fitting technique. Toward HD 119608, the cloud model derived from the high resolution optical data (5 km/s velocity resolution) can be applied to the low resolution (25 km/s) ultraviolet data. We varied the column density and added additional cloud components at higher velocities in order to fit the profiles of several of the clear and interesting interstellar lines. An example is given in Figure 25.

The profile fitting process gives the individual velocity, Doppler broadening width, and column density of each separate cloud along the line of sight. The resulting cloud column densities are listed in Table 3. The uncertainties in these values are proportional to the uncertainties in the equivalent widths, typically 20 to 30% for these data.

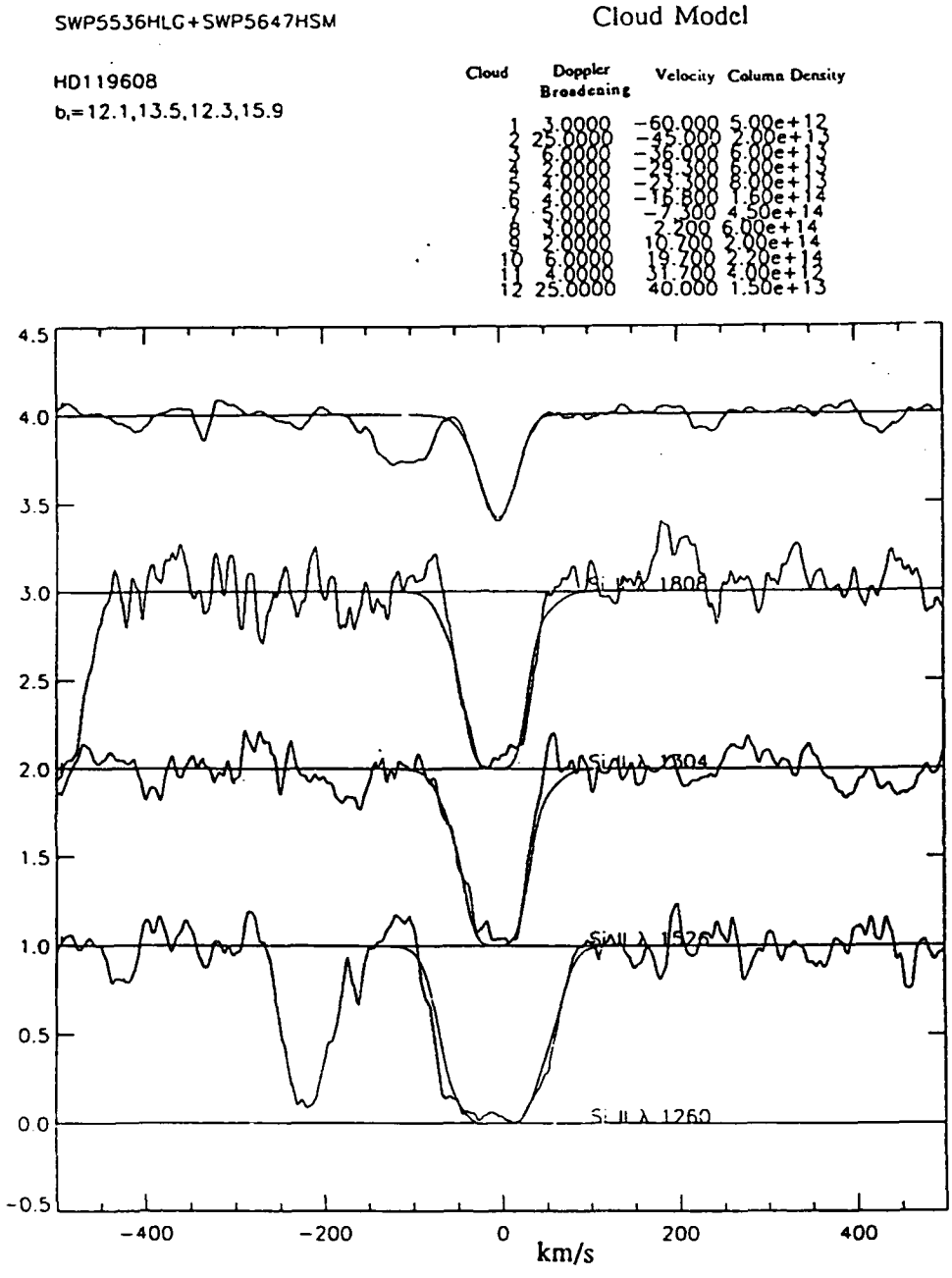

Figure 25: Profile fit of the Si II lines toward HD119608 using the cloud model from the optical as the starting model for the fitting process. The model profiles are shown with the observed lines.

Table 3: Column Densities by Profile Fitting

Star	Component	Ca II-K			Ca II-H			Ti II			
		v_{LSR} (km s^{-1})	N (10^{11} cm^{-2})	b (km s^{-1})	v_{LSR} (km s^{-1})	N (10^{11} cm^{-2})	b (km s^{-1})	v_{LSR} (km s^{-1})	N (10^{11} cm^{-2})	b (km s^{-1})	limit (10^{11} cm^{-2})
HD 119608	1	−29.3	0.2	2.0	−29.3	0.2	2.0				
	2	−23.3	0.7	4.0	−23.3	0.5	4.0	−23.3	1.0	4.0	
	3	−16.8	1.5	4.0	−16.8	2.1	4.0	−16.0	1.5	4.0	
	4	−7.3	4.0	5.0	−7.5	4.5	5.0	−7.3	3.0	5.0	
	5	2.2	6.8	3.0	2.0	7.5	3.0	2.7	6.7	5.5	
	6	10.7	0.8	2.0	10.7	1.1	2.0	10.7	0.3	2.0	
	7	19.7	9.5	6.0	19.7	9.3	5.3	21.0	10.5	7.1	
	8	31.7	2.0	4.0	30.5	2.1	2.5	34.5	1.4	4.0	
HD 117880	3	−16.8	0.5	4.0							
	4	−5.7	5.0	4.0							
	5	2.2	1.5	3.0							
	6	10.7	1.0	5.0							
HD 118246	2	−18.7	3.1	3.8							2.0
	3	−5.7	2.3	4.5							
	—	29.3	1.0	5.0							
HD 120086	1	−28.9	0.7	6.0	−27.2	0.9	6.0				1.5
	2	−18.4	4.7	3.0	−17.7	5.4	4.5	−14.2	4.7	8.0	
	3	−4.9	7.9	4.7	−4.7	7.1	3.8	−1.7	2.9	5.0	
	4	3.1	0.8	6.0	3.3	1.2	4.0				
	5	15.1	1.0	8.0		<0.7	8.0				
HD 123884	1	−29.3	0.4	2.0		<0.6	2.0				
	2	−23.3	0.9	4.0		<1.0	4.0				
	3	−16.8	2.0	4.0	−16.8	0.9	4.0				
	4	−5.7	9.0	5.0	−6.8	10.0	5.0				
	5	2.2	2.0	3.0	2.2	3.0	3.0				
	6	10.7	4.0	5.0	10.7	5.0	5.0				
	7	21.3	15.0	7.0	21.4	23.0	7.0				
	8	31.7	5.0	6.0	31.7	3.0	6.0				

Star	Ion	Component	v LSR (km/s)	b (km/s)	N (/cm2)
HD119608	Si II	1	-60.0	3	5.0e12
		2	-45.0	25	2.0e13
		3	-36.0	6	6.0e13
		4	-29.3	2	6.0e13
		5	-23.3	4	8.0e13
		6	-16.8	4	1.6e14
		7	-7.3	5	4.5e14
		8	2.2	3	6.0e14
		9	10.7	2	2.0e14
		10	19.7	6	2.2e14
		11	31.7	4	4.0e12
		12	40.0	25	1.3e13
HD119608	Zn II	1	-65.0	3	8.0e10
		2	-45.0	5.5	5.0e11
		3	-29.3	2	2.0e12
		4	-23.3	4	3.5e12
		5	-16.8	4	5.5e12
		6	-7.3	3	7.5e12
		7	2.2	3	7.0e12
		8	10.7	2	4.0e12
		9	19.7	6	3.0e12
		10	31.7	4	2.5e12
		11	45.0	4	1.0e12
HD119608	Cr II	1	-45.0	3	2.0e12
		2	-36.0	6	2.3e12
		3	-29.3	2	2.8e12
		4	-23.3	4	2.2e12
		5	-16.8	4	4.0e12
		6	-7.3	3	6.0e12
		7	2.2	3	7.0e12
		8	10.7	2	6.7e12
		9	19.7	6	5.5e12
		10	31.7	4	4.0e12

In order to compare the precision of the two methods for obtaining column density, Table 4 gives the sum of the column densities of the cloud models and the total column density derived from the curve of growth technique. These values are comparable to within their uncertainties.

Table 4: Total Column Densities by Two Methods

(N in atoms / cm^2)

HD119608	(Profile Fit)	(Curve of Growth)		
Ion	N	N	%Difference	Average
Si II	1.87 e15	1.00 e15	47	1.43 e15
Zn II	3.61 e13	1.78 e13	50	2.73 e13
Cr II	4.25 e13	5.01 e13	18	4.63 e13

VI Results

Taken together, the radio, optical and ultraviolet observations of this unusual region in our Milky Way galaxy, lead to four principal results, all of which are suggestive of a large scale flow dynamic such as a galactic chimney. First, we see a large scale outflowing cloud in neutral hydrogen emission spectra spanning a distinct region of the sky across the area from 310º to 330º galactic longitude and from about 38º to 48º galactic latitude. After we identified the only region of marked outflow in the northern galactic sky in the low resolution Bell Labs H I survey, we mapped the location at high spatial resolution using the 140 foot National Radio Astronomy Observatory radio telescope. The high resolution mapping confirms the large scale outflow of neutral hydrogen and shows fine scale structure in the motions of interstellar gas. We determine the distance limits of the outflow using high resolution optical absorption spectra of stars along the line of sight through the outflowing hydrogen region. The positive velocity components in the line profile models of singly ionized calcium appear at a height of about 1 kpc

above the galactic plane and increase in strength into the halo. The column density of the outflowing components increases from the height 3.1 kpc at HD119608 to the star HD123884, believed to be at 8.9 kpc above the plane of the galaxy. The relation between height and outflowing column density can be seen in Table 5. Although it is unlikely that the cloud extends

Table 5: Outflow Column Density with Distance

Star	Distance	Ca II N at 25km/s
117880	0.33 kpc	0
118246	1.1 kpc	1.0 e11
119608	3.1 kpc	11.5 e11
123884	8.9 kpc	20.0 e 11

that far above HD119608, this evidence certainly indicates that gas is flowing out of the plane of the galaxy to heights thousands of light years beyond the disk. The detections of the outflow feature in singly ionized titanium confirms that the observations of Ca II and H I indeed represent the same neutral cloud. Interestingly, we do not see the strong outflow of H I toward the star HD123884 which is observed in the calcium absorption toward this star. HD123884 may mark the edge of a line of sight where the accelerated cool cloud becomes ionized.

In addition to the large scale regional outflow of the gas clouds in the HD119608 line of sight, the second principal result of this study is the detection

of certain ions in the ultraviolet spectra which provide some crucial keys to unravelling the mystery of this galactic flow. Highly ionized species detected in ultraviolet absorption generally indicate hot gas. We see strong C IV in the spectra toward the stars HD119608 and BD+2 2711 and also detect the high ion Si IV. The approximate C IV / Si IV ratio from the curve of growth values of column density is 3.9 toward HD119608. While the C IV and Si IV are not unique to this line of sight, the most highly ionized species in the absorption spectrum of HD119608 is the ion N V which has not been found in the interstellar absorption spectra of any other high latitude star. Nitrogen V may be a particularly important indicator of gas temperature as it is generally believed to indicate an area of collisionally ionized gas cooling through a narrow temperature range of about 10^5 Kelvin.

While the presence of high ions is a significant result in and of itself, just as interesting is the third result: velocity trends in motion that we observe in the high ions. HD119608, HD125924 and HD121968 all show a trend of stronger absorption at infalling velocities for the high ions and outflowing for the low ions. This trend is not observed in the higher latitude star BD+2 2711, where the absorption lines are centered at zero velocity. Therefore, the flow of cold gas out of the disk of the galaxy and hotter gas into the disk occurs up to the latitude of the former stars (43 to 56º) but does not extend to the height of BD+2 2711 at 62º.

These flows are large-scale phenomena, but they are localized in a well defined region of space. The observations are consistent with a chimney scenario and provide important constraints for future theoretical models. Gas flowing out of the disk in a galactic chimney is expected to be hot, but models (eg Norman and Ikeuchi 1989) cannot confidently predict an exact

temperature range. Our observation of the high ions C IV, S IV, and especially N V flowing *toward* the disk suggests that the gas was hotter yet, perhaps 10^6 Kelvin, when originally ejected upwards. The outflowing neutral cloud that we observe is therefore not cold condensations within that chimney flow but could be a supernova shell or swept up ambient disk gas propelled upwards by a later chimney event.

The fourth principal result of this study is the strong abundance of singly ionized chromium in addition to unusually strong calcium and titanium absorption along this line of sight. All of these refractory elements condense very easily onto interstellar grains of dust leaving few atoms of the element in the gas, so the absorption line is usually very weak and indicates only a fraction of the actual number of atoms in space because most are condensed onto grains. When the grains have been destroyed by some mechanism such as the shock from a supernova or high velocity clouds (Routly and Spitzer 1952) associated with a chimney or fountain flow, the normally "depleted" elements are liberated into the gas, or "dedepleted", and can therefore cause a strong absorption line. The pattern of chromium depletion is similar to that of the optically observed Ca II and Ti II. Like Ti II, Cr II is a dominant ionization stage in regions of neutral hydrogen. From the column densities in the profile fitting technique we find that the ratio of the abundance of chromium varies from 3 to 84% of the solar abundance. Chromium is particularly enhanced in both the outflowing and infalling velocity components, again consistent with grain disruptions in infalling fountain material or in supernova shocks (Table 6).

Table 6 : Abundances of Refractory Elements

component (LSR velocity)	gas phase abundance, N(x)/N(H I) relative to the solar abundances		
	Cr II	Ca II	Ti II
-29.3	0.84	0.002	____
-23.3	0.52	0.003	0.0130
-16.8	0.17	0.002	0.056
-7.3	0.03	0.0005	0.018
2.2	0.07	0.001	0.046
10.7	0.34	0.0008	0.017
19.7	0.15	0.003	0.140
31.7	0.49	0.002	0.106

Unlike chromium, zinc does not condense easily onto grains and therefore serves as a good indicator of actual metal content of the gas (Pettini et al. 1990). Since the ionization potential of Zn II to Zn III is 17.96 eV, which is much greater than the 13.6 eV needed to ionize hydrogen, Zn II is also the dominant ionization stage in neutral hydrogen regions. The measured ratio of zinc with respect to hydrogen, Zn II / H I, is essentially its total abundance, Zn/H. Surveys of interstellar zinc to hydrogen ratios show the average value to be 2.61×10^{-8}, or 58% of the solar abundance (Harris et al. 1983). The total column density of zinc in the region of this study is average but the individual column density at the positive velocity clouds is 158% of solar and the negative velocity component is 84% of solar, while the zero velocity material has a zinc

abundance of only 23% of solar. This work is the first study of interstellar zinc abundances in individual cloud components and reveals that the zinc abundance is more complex than observed in previous general surveys. At least along this line of sight, the abundance varies significantly with velocity and may correlate with different histories of various individual clouds. Both the outflowing and infalling clouds in this region show particularly enhanced zinc, and thus high metallicity, characteristic of gas recently cycled through a supernova.

Of course, these results depend upon the continuum fitting process, the resolution of the absorption lines and the reliability of the profile fitting method. However, even if the zinc column density were reduced by a factor of two, the basic conclusions would still stand. In this case, the average zinc abundance in the positive velocity components would be 84% of the solar abundance, which is still a factor of 1.4 greater than the average interstellar value.

With the results of a strong outflowing feature with spatial and distance constraints, presence of high ions including N V, a velocity separation between high and low ions, and enhanced chromium and zinc at the positive velocity components, we have accomplished our preliminary objectives of exploring the candidate chimney region in space, distance, velocity and ionization.

VII Conclusions

No static halo model can explain our very dynamic observations. Strong activity is accelerating material causing a separation in the velocity of the low and high ions. Definite trends have been noted in space, distance, velocity, and ionization. Enhanced chromium and calcium indicated grain destruction associated with a shocked region while high zinc abundance reveals high metallicity characteristic of gas recently recycled through a supernova. The strong feature of outflowing neutral hydrogen and low ions is consistent with the swept up shell of a supernova remnant or could be an unrelated feature. The ultraviolet results are consistent with a very hot chimney model with a very long cooling time in which the gas would, *in fact, have to be too hot to* observe with our methods on the way out of the disk (perhaps one million degrees Kelvin) and we see the returning fountain flow only when the gas has cooled to the relatively cooler "high" ions that we see at predominantly infalling velocities. If this local phenomenon is typical of the galaxy as a whole, then the cycling of gas between the stars in the disk and the halo must play an important role in the dynamics and evolution of the Milky Way.

Acknowledgements

We wish to express our tremendous gratitude to:

K. D. Kuntz of the Space Telescope Science Institute for his work in writing and revising all of the software used for absorption line analysis (KDAF) and H I contour mapping (HI-IDL) in this project and for useful discussions.

F. J. Lockman of the National Radio Astronomy Observatory for instruction and advice on H I observations and analysis.

G. Sonneborn of NASA Goddard Space Flight Center for his ultraviolet spectral classification of the stars we observed.

The staffs of the National Radio Astronomy Observatory and the International Ultraviolet Explorer.

The National Radio Astronomy Observatory is operated by Associated Universities, Inc., under contract with the National Science Foundation.

The International Ultraviolet Explorer Satellite is sponsored and operated by the National Aeronautics and Space Administration, by the Science Research Council of the United Kingdom and by the European Space Agency.

References

Albert, C.E. 1983, Astrophysical Journal, 272, 509.

Albert, C.E., Blades, J.C., Lockman, F.J. , Morton, D.C., and Proulx, M. 1992, in preparation.

Bidleman, W.P. 1988, Publications of the Astronomical Society of the Pacific, 100, 1084.

Bregman, J.N. 1980, Astrophysical Journal, 236, 577.

Chevalier, R. and Fransson, C. 1984, Astrophysical Journal Letters, 209, L105.

Danly, L. 1989, Astrophysical Journal, 342, 785.

Danly, L., Lockman, F.J., Meade, M.R., Savage, B.D. 1992, Astrophysical Journal Supplement, in press.

de Boer, K.S., Lenhart, H., Van der Hucht, K.A., Kunperman, T.M., Kondo, Y., and Bruhweiter, F.C. 1986, Astronomy and Astrophysics, 157, 119.

Harris, A.W., Bromage, G.E. and Blades, J.C. 1983, Monthly Notices of the Royal Astronomical Society, 203, 1225.

Harris, A.W., and Mas Hesse, J.M. 1986, Monthly Notices of the Royal Astronomical Society, 220, 271.

Hill, P.W. 1970, Monthly Notices of the Royal Astronomical Society, 150, 23.

Houk, N. 1982, Ann Arbor, Dept of Astronomy, Univ. Michigan, Vol. 3.

Jenkins, E. 1986, Princeton University Observatory, POP-185.

Morgan, W.W., Keenan, P.C., and Kellman, E. 1943, An Atlas of Stellar Spectra (Chicago: Univ. Chicago Press).

Morton, D.C. 1991, Astrophysical Journal Supplement, 77, 119.

Munch, G., and Zirin, H. 1961, Astrophysical Journal, 133, 11.

Norman, C. and Ikeuchi, S. 1989, Astrophysical Journal, 345, 372.

Pettini, M., Boksenberg, A. and Hunstead, R. W. 1990, Astrophysical Journal, 348, 48.

Rountree, J. and Sonneborn, G. 1990, Astrophysical Journal, 369, 515.

Sonneborn, G., Oliversen, N.A., Imhoff, C. L., Pitts, R.E., and Holm, A.V. 1987, International Ultraviolet Explorer NASA Newletter, 32.

Spitzer, L. 1963, Diffuse Matter in Space (New York: Interscience Publishers).

Spitzer, L. 1978, Physical Processes of the Interstellar Medium (New York: John Wiley and Sons).

Stark, A.A., Gammie, C.F., Wilson, R.W., Bally, J., Linke, R.A., Heiles, C. and Hurwitz, M. 1992, Astrophysical Journal Supplement, 79, 77.

Stetson, P. and Fitzgerald, H.P., 1985, Astronomical Journal, 90, 1060.

Tobin, W. 1985, Astronomy and Astrophysics Supplement, 60, 459.

Williams, D.R. 1972, Astronomy and Astrophysics Supplement, 8, 505.

Appendix A

Neutral Hydrogen Emission Contour Maps

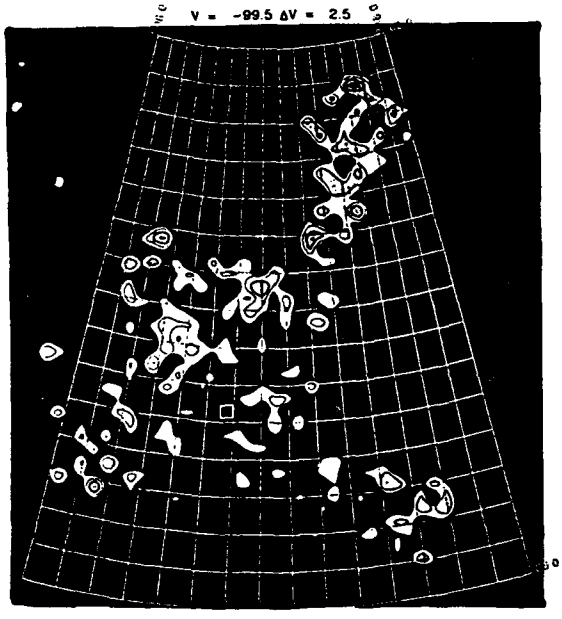

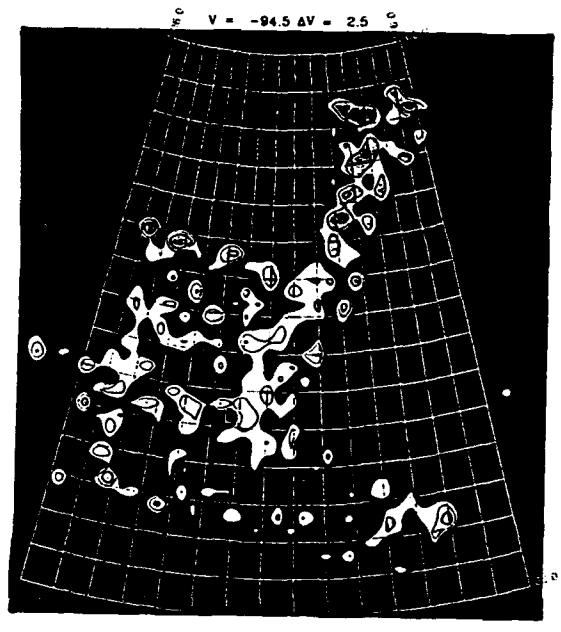

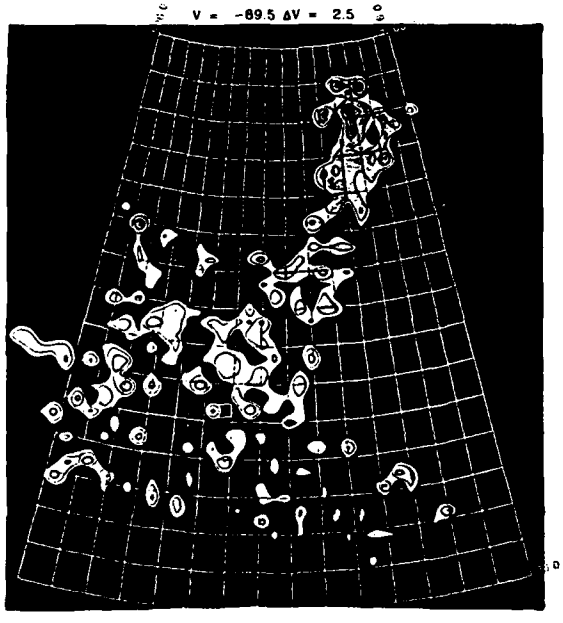

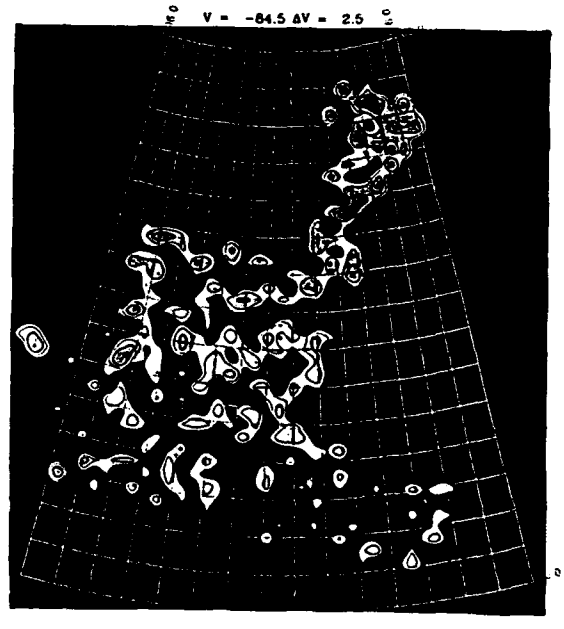

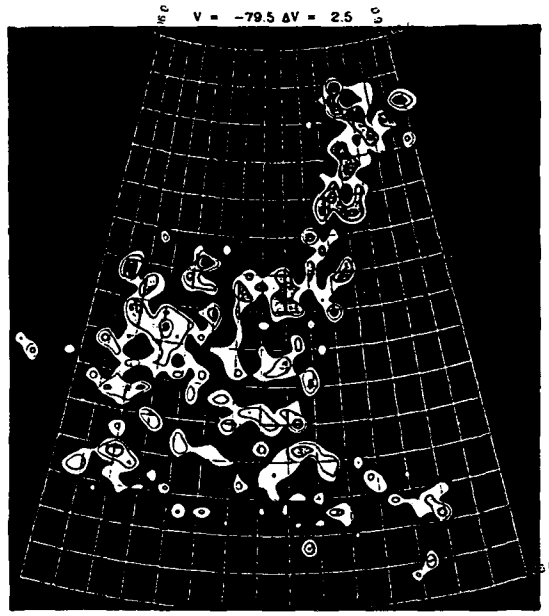
V = -79.5 ΔV = 2.5

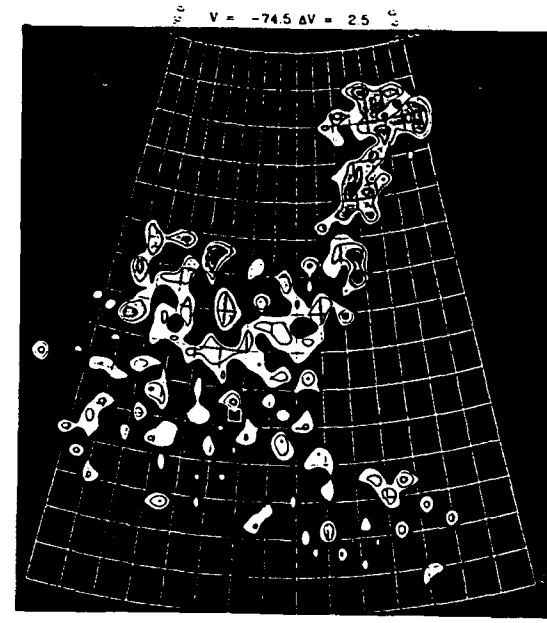
V = -74.5 ΔV = 2.5

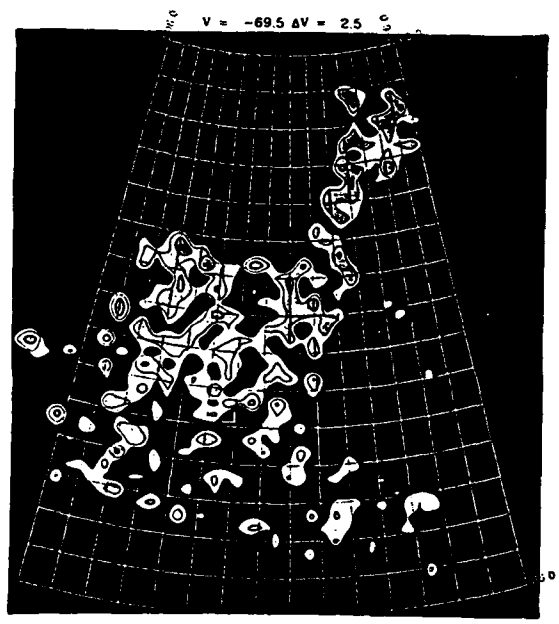
V = -69.5 ΔV = 2.5

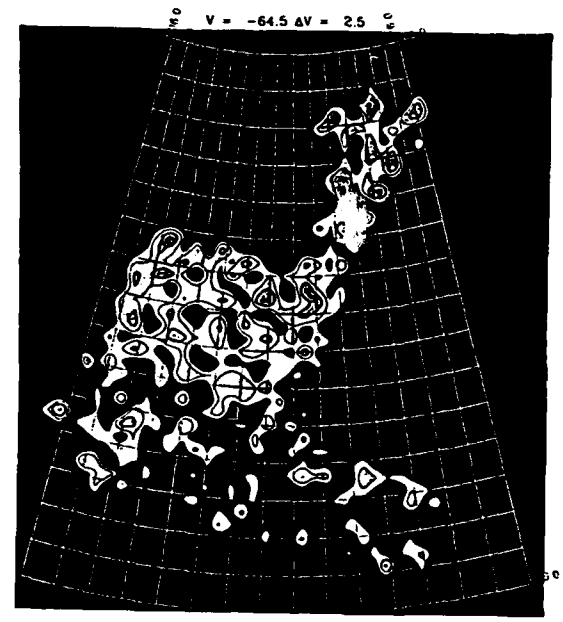
V = -64.5 ΔV = 2.5

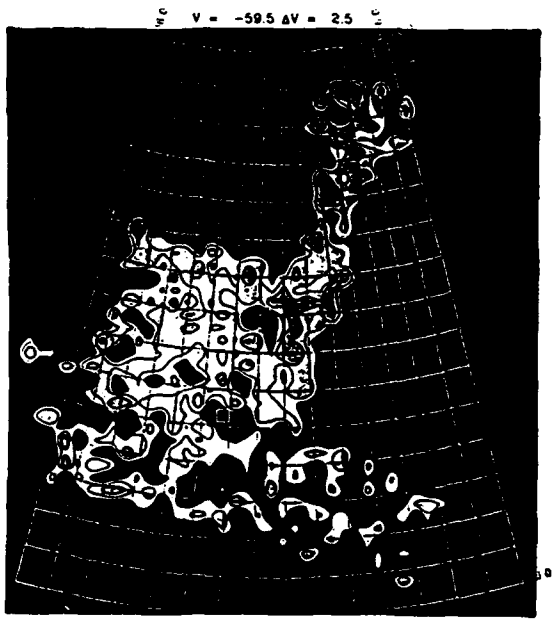
V = -59.5 ΔV = 2.5

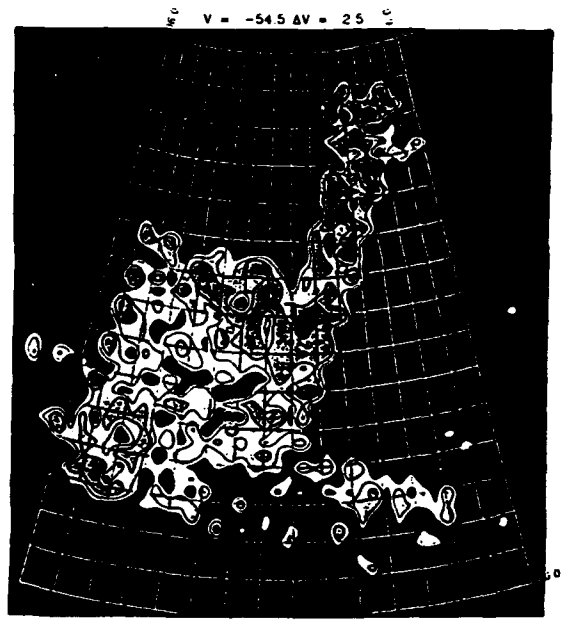
V = -54.5 ΔV = 2.5

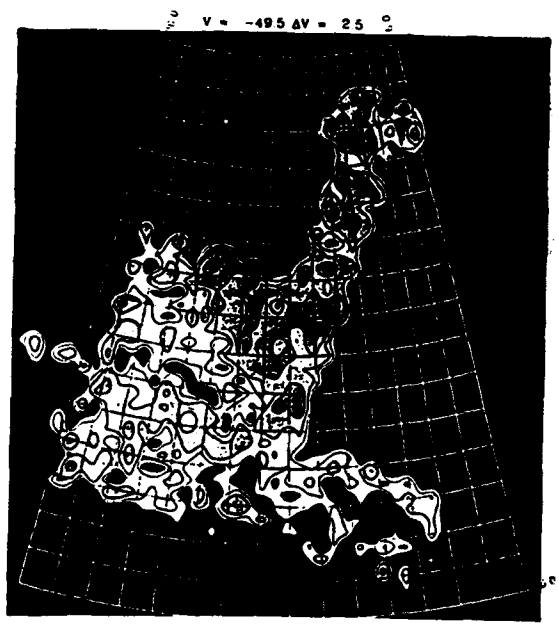
V = -49.5 ΔV = 2.5

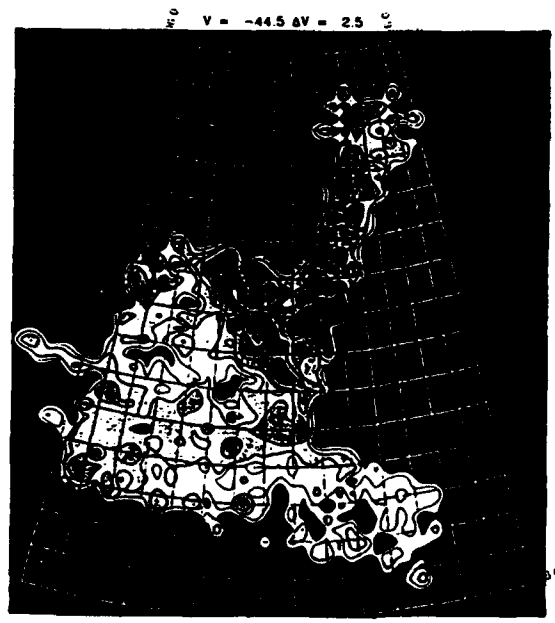
V = -44.5 ΔV = 2.5

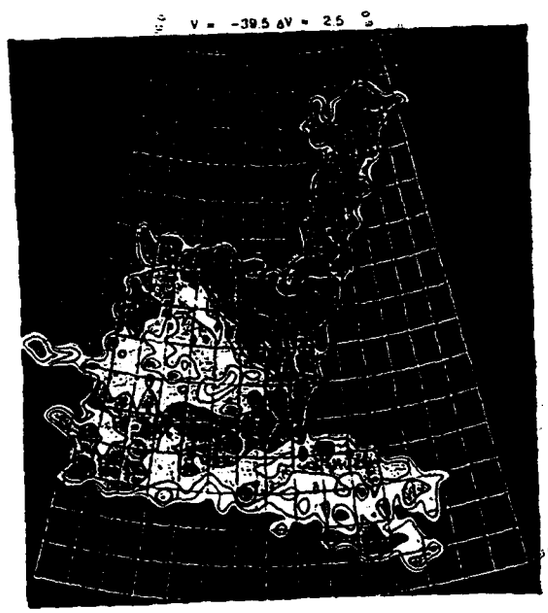
V = -39.5 ΔV = 2.5


V = -34.5 ΔV = 2.5

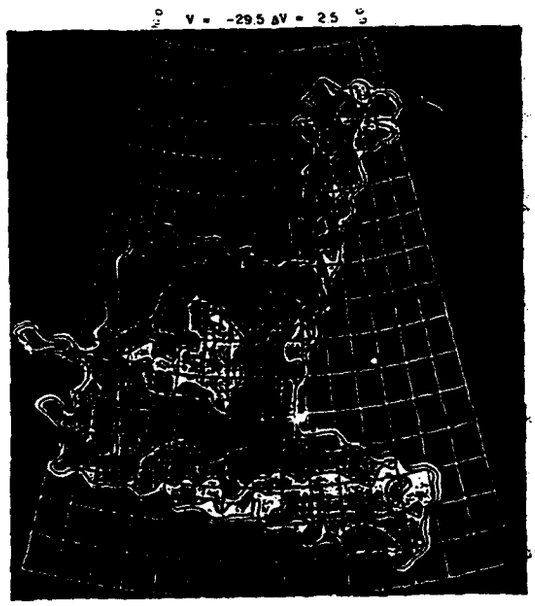
V = -29.5 ΔV = 2.5

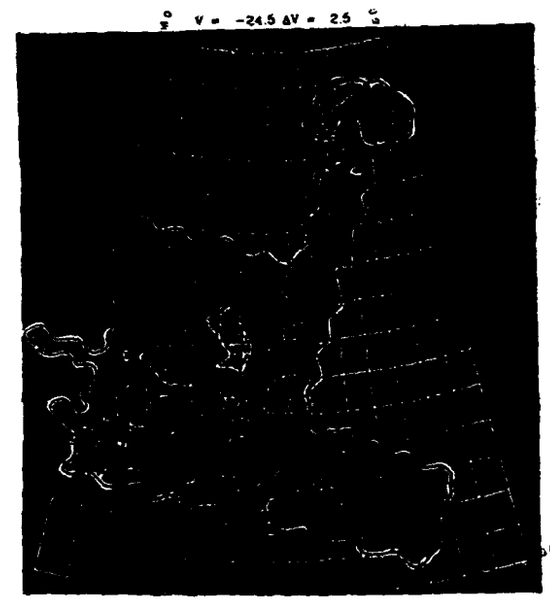
V = -24.5 ΔV = 2.5

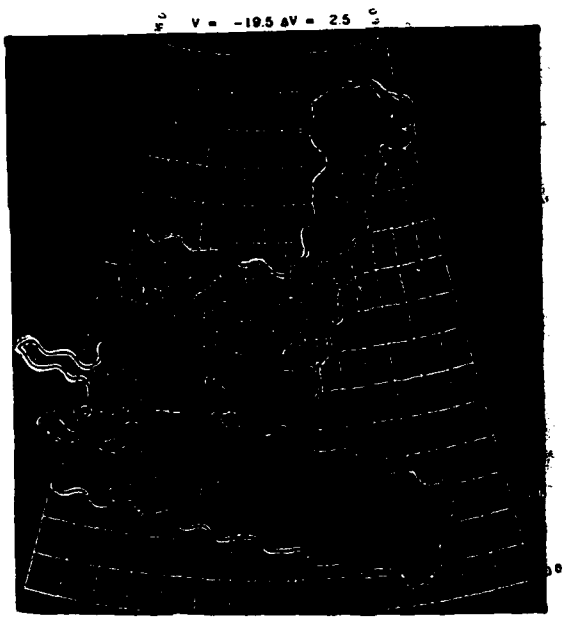
V = -19.5 ΔV = 2.5

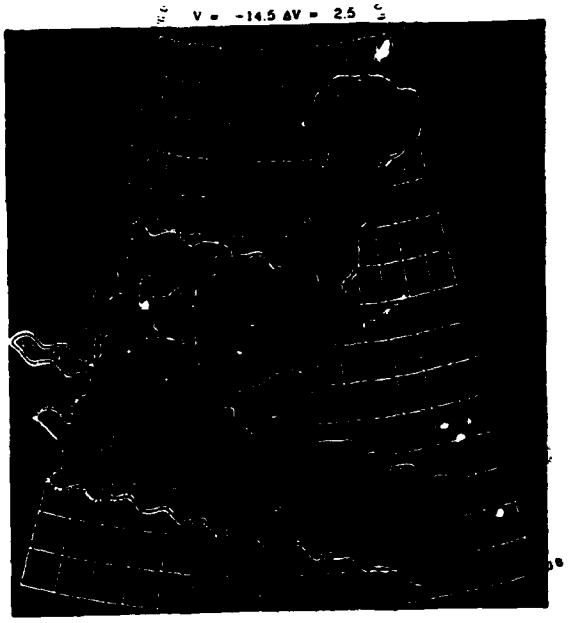
V = -14.5 ΔV = 2.5


V = -9.5 ΔV = 2.5

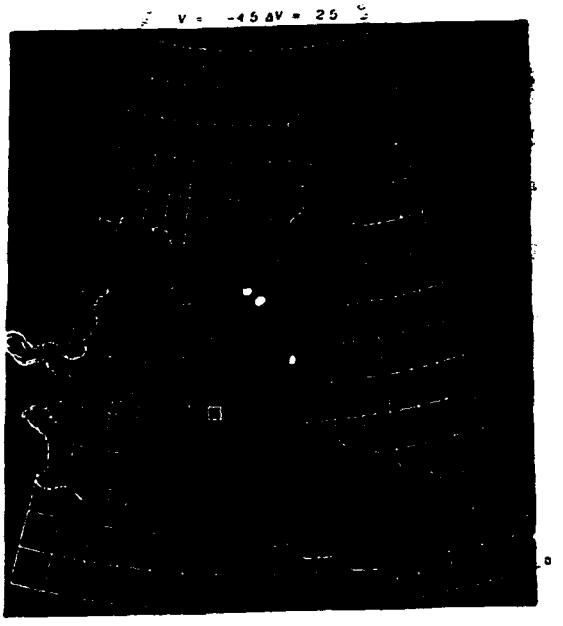
V = -4.5 ΔV = 2.5


V = 05 ΔV = 25


V = 55 ΔV = 25

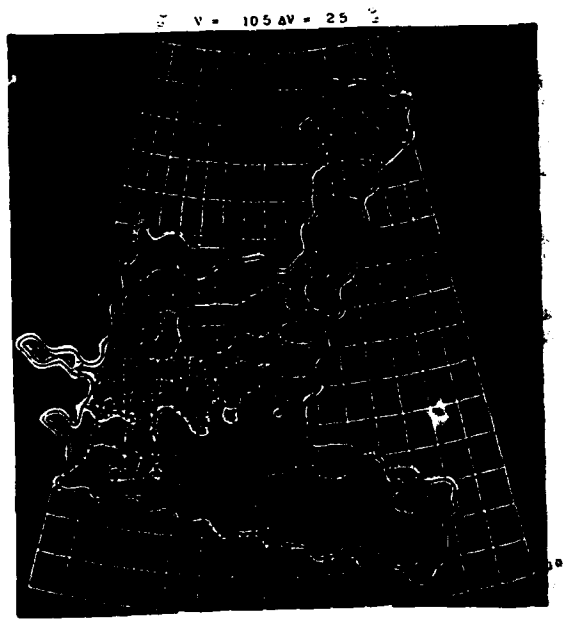
V = 105 ΔV = 25

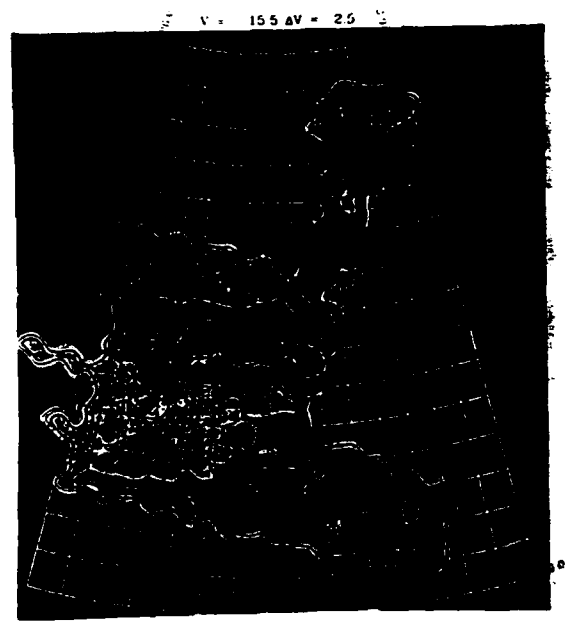
V = 155 ΔV = 25


V = 20.5 ΔV = 2.5

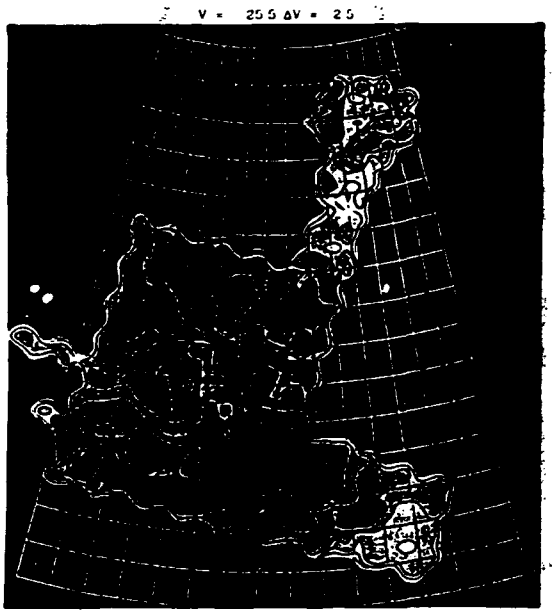
V = 25.5 ΔV = 2.5


V = 30.5 ΔV = 2.5


V = 35.5 ΔV = 2.5

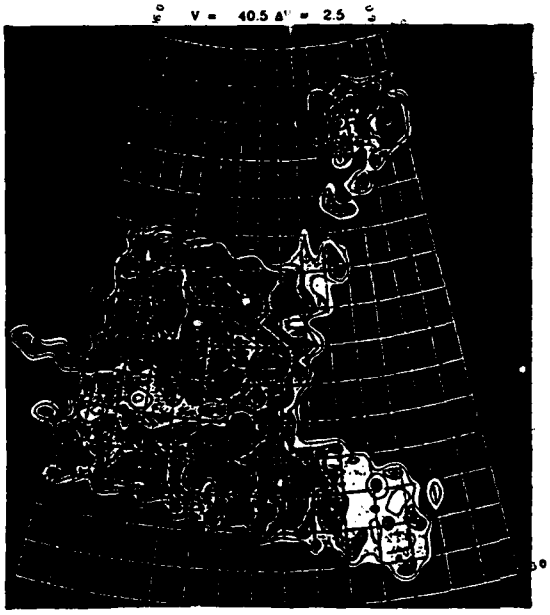
V = 40.5 ΔV = 2.5

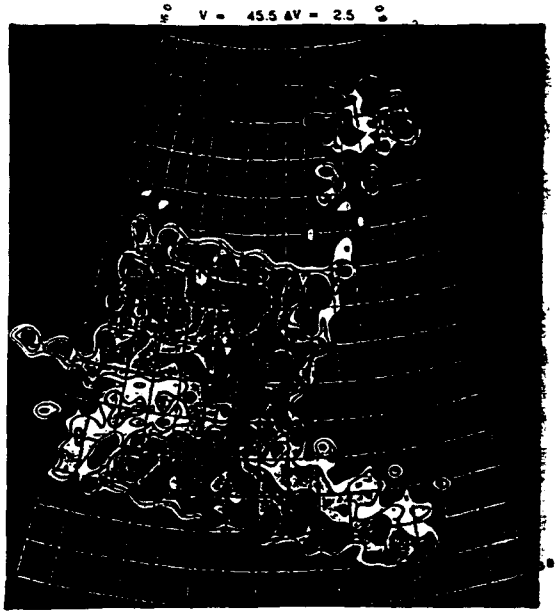
V = 45.5 ΔV = 2.5

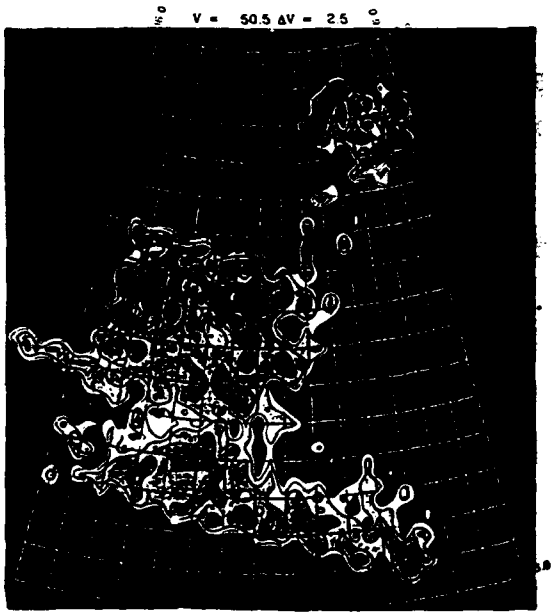
V = 50.5 ΔV = 2.5


V = 55.5 ΔV = 2.5

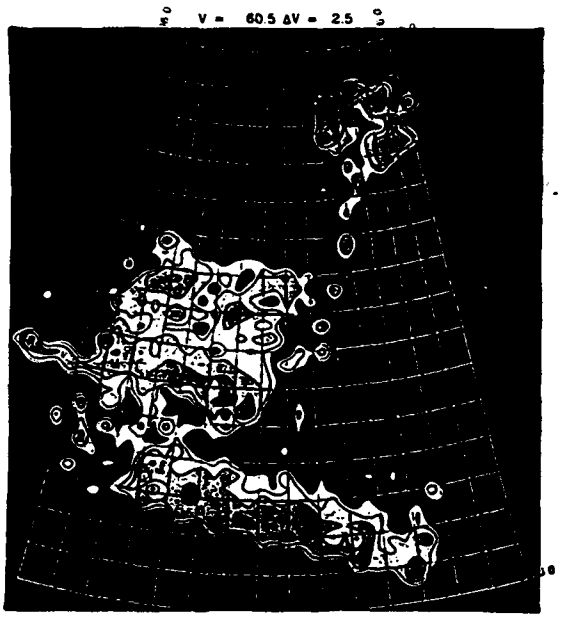
V = 60.5 ΔV = 2.5

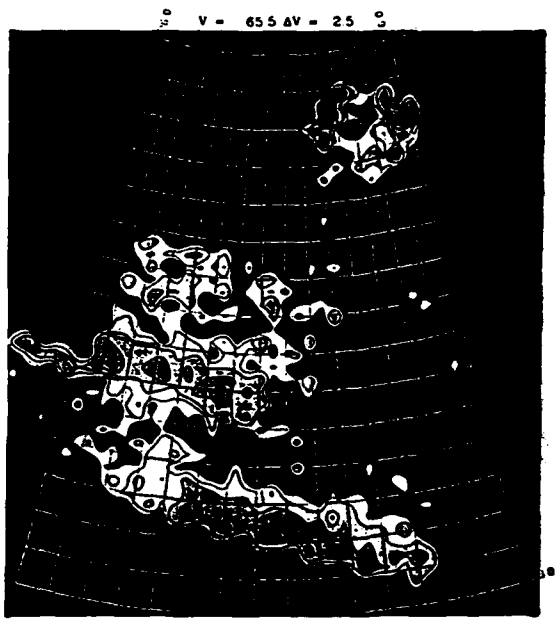
V = 65.5 ΔV = 2.5

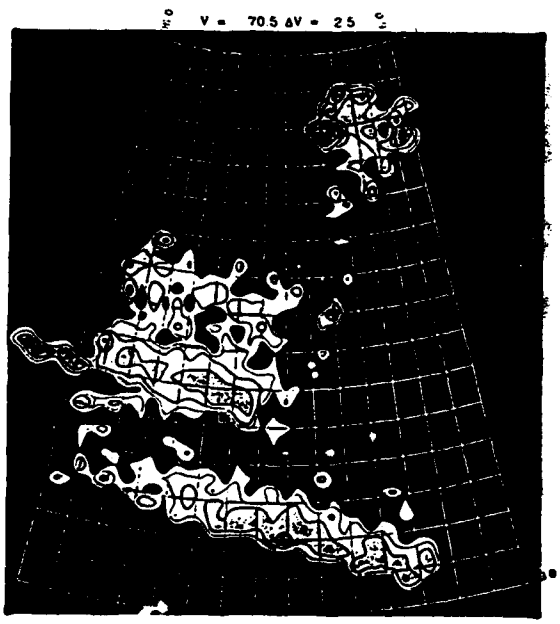
V = 70.5 ΔV = 2.5

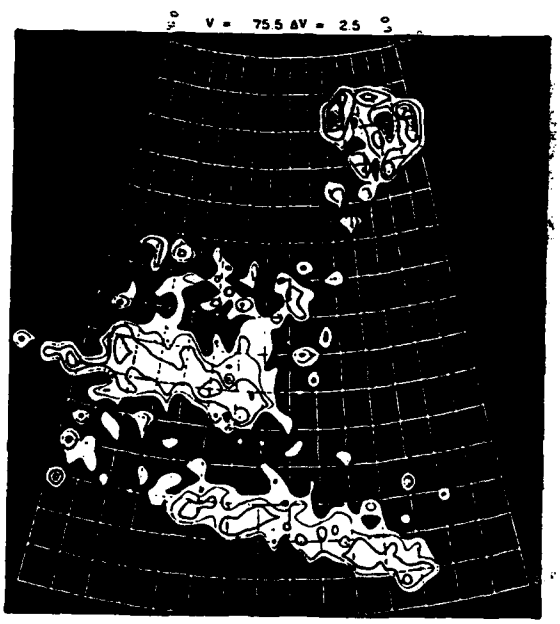
V = 75.5 ΔV = 2.5

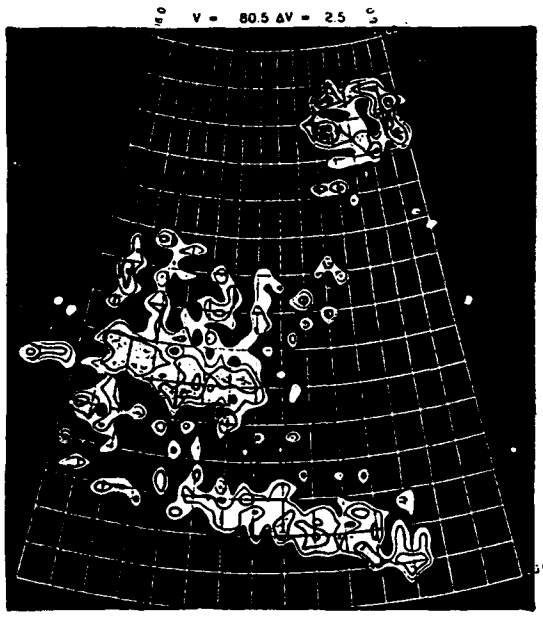
V = 80.5 ΔV = 2.5

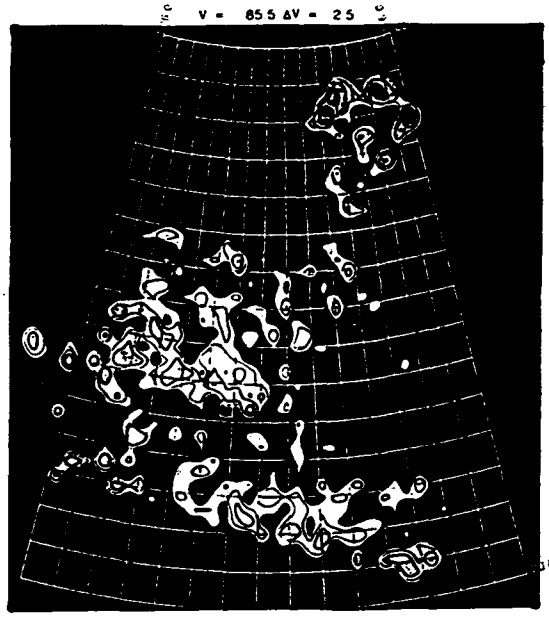
V = 85.5 ΔV = 2.5

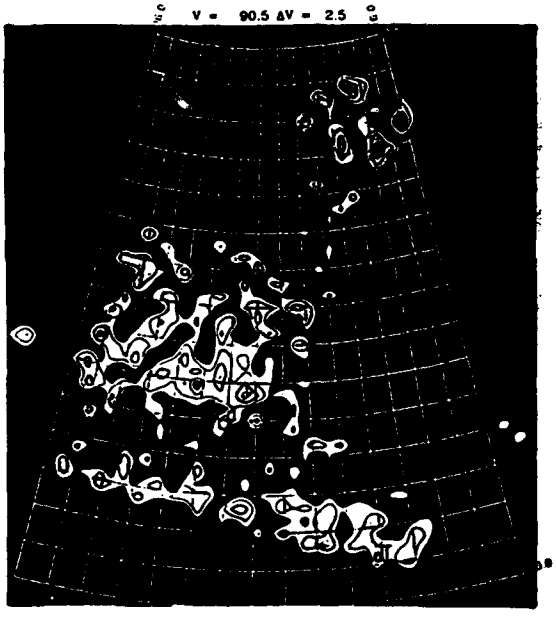
V = 90.5 ΔV = 2.5

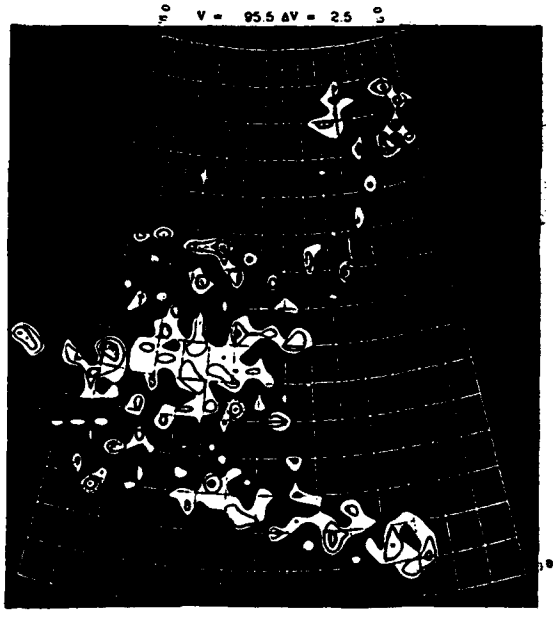
V = 95.5 ΔV = 2.5

Appendix B

Atomic Line Data File

Line	Wavelength	Oscillator Strenth (F)	Upper	Lower	Order
N I	1199.5496	0.133000	6	4	115
SI III	1206.500	1.660000	3	1	115
SI III	1206.500	1.660000	3	1	114
N V	1238.821	0.152000	4	2	112
N V	1238.821	0.152000	4	2	111
N V	1242.804	0.075700	2	2	111
S II	1250.584	0.005350	2	4	110
S II	1253.811	0.010700	4	4	110
S II	1259.519	0.015900	6	4	110
S II	1259.519	0.015900	6	4	109
SI II	1260.4221	0.960000	4	2	109
Si III	1294.540	0.000000	0	0	107
Si III	1294.540	0.000000	0	0	106
O I	1302.1685	0.048600	3	5	106
Si II	1304.3702	0.147000	2	2	106
C II	1334.5323	0.118000	4	2	103
C II*	1335.7077	0.118000	10	8	103
Si IV	1393.755	0.528000	4	2	99
Si IV	1402.770	0.262000	2	2	98
Si III	1417.243	0.000000	0	0	97
Si II	1526.7066	0.230000	2	2	90
C IV	1548.195	0.194000	4	2	89
C IV	1550.770	0.097000	2	2	89
Fe II	1608.4511	0.062000	8	10	86
Al II	1670.7874	1.880000	3	1	83
Al II	1670.7874	1.880000	3	1	82
Si II	1808.0126	0.005500	4	2	76
Al III	1854.7164	0.539000	4	2	74
Al III	1862.7895	0.268000	2	2	74
C I	1656.928	0.136000	3	1	83
C I	1560.310	0.081000	3	1	88
C I	1280.135	0.027800	3	1	108
O I*	1304.858	0.048500	3	3	106
O I**	1306.029	0.048500	3	1	106
Si II	1193.289	0.500000	2	2	115
Si II	1193.289	0.500000	2	2	116
Si II	1190.416	0.250000	4	2	116
N II	1751.910	0.040000	8	6	79
N II	1741.549	0.067900	6	6	79
N II	1709.600	0.047000	6	6	81
N II	1454.842	0.051500	6	6	95
N II	1370.132	0.130000	4	6	100
N II	1370.132	0.130000	4	6	101
Zn II	2062.005	0.202000	2	2	67
C I	1277.245	0.156000	3	1	108
Cr II	2055.596	0.109000	8	6	67
Zn II	2025.483	0.412000	4	2	68

The atomic line data file gives the parameters about a given line necessary for modeling it. The oscillator strengths and numbers of upper and lower transitions are from Morton 1991. The order is the line on the photowrite that contains the wavelength of interest.

Appendix C: Curve of Growth Theory

The relationship between the equivalent width and the column density is the curve of growth.

Equivalent width is defined as the area under the absorption line and, if the background is normalized to unity, it is expressed in units of wavelength, or Angstroms. Mathematically, equivalent width is written as:

$$W_\lambda = \int \left(1 - \frac{I_\nu}{I_\nu(0)?}\right) d\lambda.$$

where $I_\nu(0)$ is the background or continuum intensity and I_ν is the intensity at each point along the absorption line. $d\lambda$ is the small change in wavelength across the line, so the sum of the normalized line depth $(1-I_\nu/I_\nu(0))$ times the increment in width equals the area under the line.

Equivalent width relates to the optical depth, τ_ν, of the cloud by the expression:

$$W_\lambda = \int \left(1-e^{-\tau_\nu}\right) d\nu$$

where the integral is now expressed as a function of frequency rather than wavelength. The optical depth of a line is a measure of the atomic element's absorption across a line profile $\varphi(\nu)$:

$\tau = N_j \, s \, \varphi(\nu)$ where N_j is the number of atoms in the lower energy state along a line of sight

$s = 2.65\times10^{-2} \, f_{jk}$ where f_{jk} is the oscillator strength, a measure of the probabity of the transition

In a weak line, $\tau_\nu << 1$, we can expand the exponent so that

$$\frac{W_\lambda}{\lambda} = \int \tau_\nu d\nu = 8{,}85\times10^{-13} \, f_{jk} \, N_j$$

In the case of the weak line, then, the equivalent width over the wavelength is directly proportional to the column density and the oscillator strength. This is the "linear" portion of the curve of growth and the shape of the line is determined by Doppler broadening.

For stronger lines, the optical depth is large and the amount of energy absorbed is no longer proportional to optical depth. The line is said to be saturated and the observed equivalent width does not change significantly over a wide range of column density. This is the "flat" portion of the curve of growth. In this case, the curve depends on the detailed line profile and can be written as :

$$W_\lambda = 2\,\beta\,F(C)$$

where:

$$\frac{\beta^2}{\nu^2} = \frac{2kT}{m_a c^2}$$

$$F(C) \equiv \int \left(1 - e^{-C(e^{(-x^2)})}\right) dx$$

$$C = \frac{N_j s}{\sqrt{\pi}\,\beta}$$

Finally, when the optical depth becomes very large, radiation damping wings become important and ultimately dominate the line shape. This is the "square root" portion of the curve of growth since, in this limit,

$$W = 2\left(N_j\, s\gamma\right)^{\frac{1}{2}}$$

where γ, a measure of the width of the upper level of the transition, is determined by the Einstein A coefficients:

$$\gamma = \frac{1}{4\pi}\sum_j A_{kj}$$

Combined, these equations result in the theoretical curve-of-growth shown schematically in Figure A.1.
As described in the text, the shift between observed data, plotted as log (W_λ / λ) versus log ($f_{jk}\,\lambda$) and the theoretical curve of growth gives the column densities of the observed lines. Table A.1 lists the observed equivalent widths of the ultraviolet absorption lines and Figure A.2 illustrates the curve of growth analysis. The resulting column densities were presented in text (Table 2).

Table A.1 : Equivalent Widths

Wavelength	W HD119608	W BD+2 2711	W HD123884
Si II 1808	0.140	0.515	0.241
1526	0.407	0.353	0.407
1304	0.348	0.183	
1260	0.561	0.406	
S II 1250	0.185	0.0059	
1253	0.279	0.131	
1259	0.280	0.159	
Zn II 2026	0.322	0.0669	0.260
2062	0.183	0.034	0.173
Cr II 2065	0.085	0.027	0.125
2062	0.165	0.0476	0.226
2055		0,075	
Ni II 1751		0.0822	0.234
1741			0.182
1709		0.102	0.351
1454		0.039	
C IV 1548	0.168	0.375	
1550	0.0968	0.178	
Si IV 1393	0.194		
1407	0.0896		
N V 1238	0.115		

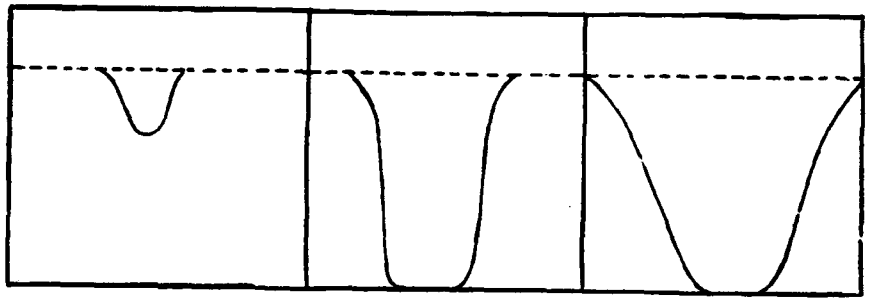

Figure A.1: Schematic example of weak, saturated, and damped lines.

Figure A.2: Fitted Curves of Growth